NERC Scientific Support and Facilities
Ion Microprobe Facility

University of Edinburgh

NERC Ion Microprobe Facility

2021-2022 Annual Science Report

Ion Microprobe Facility
School of Geosciences
Grant Institute
Kings Buildings
James Hutton Road
Edinburgh
EH9 3FE

https://www.ed.ac.uk/geosciences/about/facilities/all/ionprobe

Contents

18	Maclennan J.	Compositional profiles in plagioclase macrocrysts from the Fagradalsjall CE2021 eruption, Iceland	33
19	McMahon S., H. Drake, J. Parnell, C. Heim & A. Boyce	Life in deep fractures: evidence from Scandinavian boreholes [pilot study][EMBARGO]	35
20	Melekhova E. & J. Blundy	Basaltic andesite derived by mantle melting beneath Kluchevskoy volcano, Kamchatka	37
21	Chetan N., S. Large, E. Brugge, J. Wilkinson & Y. Buret	Apatite inclusions in zircon reveal water-saturated, crystal-rich magma reservoirs beneath porphyry copper deposits	39
22	Peck V.L.	Oxygen isotopes of laminated microspheres from the South Falkland Sediment Drift [pilot study]	41
23	Price D. & I.B. Butler	Generating economic rare earth element deposits through hydrothermal fluid-rock interactions [pilot study]	43
24	Price D. & I.B. Butler	Generating economic rare earth element deposits through hydrothermal fluid-rock interactions	45
25	Smith V., M. Humphreys, R. Isaia & J. De Hoog	Insights into the volatile evolution of the Campanian Ignimbrite magmatic system using apatite compositions	47
26	Taracsák Z., T.A Mather, T. Plank, A. Auippa, D.M. Pyle	Sulfur cycling at subduction zones: sulfur isotopic composition of Aleutian Island melt inclusions	49
27	Voigt A. & M. Cassidy	H_2O solubility in trachydacite melt [pilot study]	51
28	Wong K., D. Ferguson, P. Wieser, D. Morgan, M. Edmonds, A. Z. Tadesse, G. Yirgu, J. Harvey, S. Hammond	Crustal intrusion of basaltic magmas in the Main Ethiopian Rift	53

In-situ $\delta^{34}S$ measurements of S-rich feldspathoid minerals: investigations into the origin of sulphur at the Cameroon Volcanic Line

S. Baldwin[1], A. Boyce[2], L. Kirstein[1] & G.Fitton[1]

[1]School of GeoSciences, University of Edinburgh, Edinburgh EH9 3JW, UK
[2]Scottish Universities Environment Research Centre, East Kilbride G75 0QF, UK

Brief overview

The authors of this report applied for one day of time to use the EIMF (Edinburgh ion microprobe facility) in order to measure in-situ $\delta^{34}S$ compositions of haüyne and nosean feldspathoid crystals in lavas from Etinde, a volcano of the Cameroon Volcanic Line. A key goal was to investigate whether these crystals exhibit zonation in their $\delta^{34}S$ values, as the result would be informative for wider research into the origin and behaviour of magmatic sulphur at Etinde.

Results, discussion and ongoing work

Overall, 133 measurements of in-situ $\delta^{34}S$ values were obtained across crystals of haüyne and nosean from two thin sections of Etinde lavas (samples C218 and C228). A sample switch occurred between these two samples, potentially changing the conditions of the chamber and as such the absolute $\delta^{34}S$ values cannot be used, though the relative $\delta^{34}S$ values are informative.

The data indicate that there is no notable zonation of $\delta^{34}S$ across the haüyne and nosean crystals. We hence inferred that crystallisation of haüyne and nosean does not itself strongly fractionate S-isotopes.

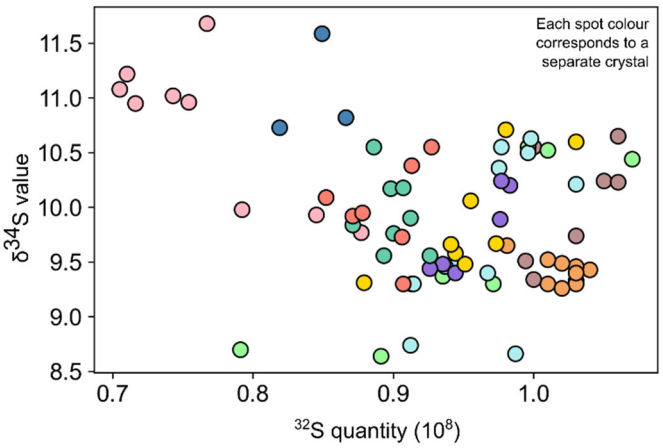

Fig. 1. The $\delta^{34}S$ value measured for each phenocryst from lava C228 plotted against the ^{32}S quantity measured used the ion microprobe to test for matrix effects.

Finding homogenous $\delta^{34}S$ compositions across crystals did not allow us to discern between hypotheses two and three in our original proposal but further lab work with collaborators in St. Andrews has since aided our understanding of the systematics of sulphur isotopes at Etinde.

Matrix effects can be problematic for isotope work and we ensured these were thoroughly investigated. The lack of a correlation between $\delta^{34}S$ value and measured quantity of ^{32}S (**Figure 1**) supports the idea that matrix effects are not imparting extensive bias to the data. Further work using a recently obtained EPMA dataset about the chemistry of these phenocrysts will contribute to our understanding of the extent of matrix effect bias in the dataset.

Copper enrichment in arc magmas in Java, Indonesia

N.D. Barber[1,2*], M. Edmonds[1], S. Baldwin[3], F. Jenner[4], H. Williams[1], H.E. Wibowo[5] & A. Harijoko[5]

[1] Department of Earth Sciences, University of Cambridge, UK. *ndb38@cam.ac.uk
[2]Department of Earth and Planetary Sciences, McGill University, Montréal, QC, Canada
[3]School of Geosciences, University of Edinburgh, Edinburgh EH9 3JW, UK
[4]School of Environment, Earth and Ecosystem Sciences, The Open University, MK7 6AA, UK
[5]Department of Geological Engineering, Universitas Gadjah Mada 55281. Yogyakarta, Indonesia

Background and Rationale

Copper, sourced from porphyry deposits formed in arc settings, is a critical resource for the burgeoning green economy [1]. The processes that shape the copper contents of magmas is well understand in economic geology and are increasingly being investigated in active volcanic settings. Assessing the impact of degassing, volatile contents, and storage depths for magmas on magamtic copper contents is of vital importance in developing a cohesive framework that links modern volcanism with the extinct products of such activity, which we currently mine for metallic resources.

To address this need, we use a combination of Raman spectroscopy, secondary ion mass spectrometry (SIMS), and electron microprobe analysis (EMPA) on olivine- and pyroxene-hosted melt inclusions (MIs) from three volcanic centers in Java, Indonesia: Galunggung (West Java), Slamet and its scoria cone Loyang (Central Java), and Bawean (Java Sea) (**Figure 1**). Java's volcanoes are known to have some of the highest H_2O contents ever measured in olivine-hosted MIs [2], a well-documented and violent history of major eruptions - including a VEI 4 eruption at Galunggung in 1982 [3] and VEI 2 eruption at Slamet in 2014 [4] - and some promising prospects for porphyry prospects (**Figure 1**; [5]).

We sent our samples to the NERC Ion Probe facility to have their melt inclusions measured remotely in December 20-January 2021. Several of the SIMS-measured melt inclusions contained previously measured CO2 densities thanks to Raman spectroscopy. Raman measured CO2 densities in melt inclusion-hosted vapor bubble have been shown to significant increases in total estimated CO2 contents vastly increasing estimated storage pressures from melt inclusion barometry [6]. These measurements should provide us with an idea of how deeply these magmas were stored; this variable is believed to have a crucial role on when copper can be optimally released for either ore mineralization of metal degassing during eruptions [7].

Results and Discussion

A total of 68 SIMS measurements were made, 42 of those on olivine hosted melt inclusions. This forms roughly a quarter of the total number of melt inclusions measurements we intend to make with the remainder of our SIMS time. Each of those melt inclusions were subsequently measured by EMPA and corrected both for post-entrapment crystallization (PEC) [8] and vapor bubble CO_2 density [6].

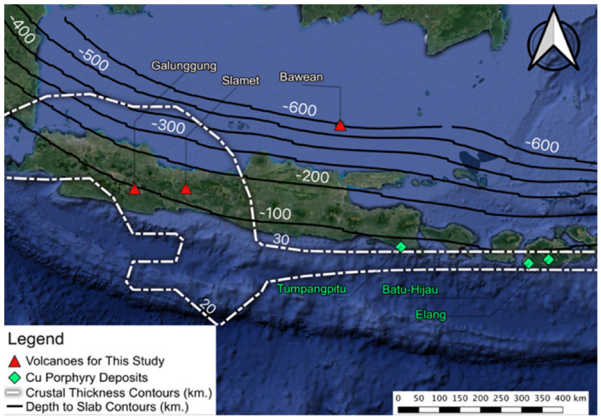

Fig. 1. Map showing the volcanoes (red triangles) from which our samples were collected (Galunggung, Slamet, and Bawean) in Java, Indonesia. Also shown are globally significant Cu porphyry deposits (green diamonds). Slab-depth contours themselves at 10 km.

Figure 2a shows the core composition of those olivine's hosting the melt inclusions – most notable is that discordance between Slamet and its scoria cone Loyang, whose olivine's seem to be sourced from a much more primitive parental melt. Melt inclusions hosting olivine also seem to be more primitive than their host crystals (**Figure 2b**). Measured melt compositions were corrected to a 1200 degree C, 3000 bar, +1 delta NNO starting composition, showing a degree of PEC of

between 3.7 and 30%. **Figure 3** shows the calculated entrapment pressures for Slamet and Loyang hosted melt inclusions. Both volcanoes are believed to share a magmatic source and can tap magmas over 12 km into the crust. Galunggung and Bawean entrapment calculations are ongoing.

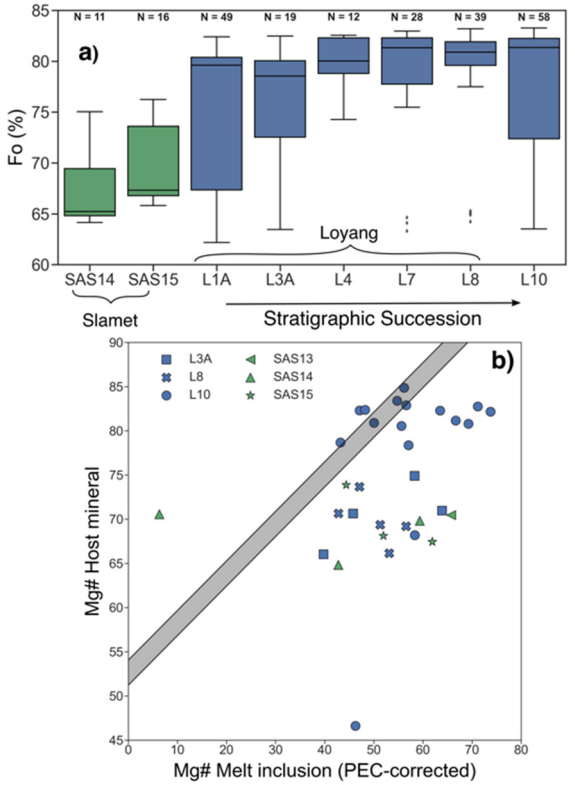

Fig. 2. a) Forsterite content (Fo) of olivines from Slamet and Loyang, including those crystals carrying SIMS-measured melt inclusions. b) Chemistry of olivine-hosting melt inclusions and their melt inclusion glass chemistry, showing disequilibrium.

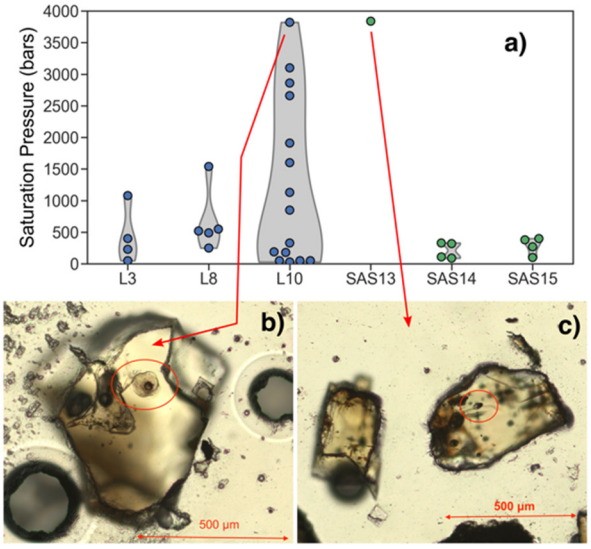

Fig. 3. Estimated entrapment pressures based on SIMS-measured H_2O and CO_2 conetns of olivine and pyroxene hosted melt inclusions. Pressures estimated using MagmaSat from VESICal. All volatile contents corrected for PEC [8].

References

[1] N. Arndt et al. (2017) Geochemical Perspectives (543)
[2] N. Vigouroux et al. (2012) Geochemistry, Geophysics, Geosystems 13(9)
[3] T.W. Sisson and S. Bronte (1998) Nature (391)
[4] A. Harijoko et al. (2021) Journal of Volcanology and Geothermal Research (418)
[5] A. Maryono et al. (2018) Economic Geology (113)
[6] P. Wieser et al. (2022) Earth and Space Science (9)
[7] N.D. Barber et al. (2021) Geochimica et Cosmochimica Acta (307)
[8] L.V. Danyushevsky et al. (2011) Geochemistry, Geophysics, Geosystems (12)

Metal evolution in basaltic melts undergoing ascent-driven degassing

J.Blundy[1], B. Kunz[2] & F. Jenner[2]

[1]Department of Earth Sciences, University of Oxford, Oxford OX13AN
[2]School of Geography and Geosciences, Open University, Milton Keynes MK

Background

Significant fluxes of metals have been measured at basaltic volcanoes worldwide across a wide range of tectonic settings [1]. These metals emissions, integrated globally, exceed the global mined flux each year for all metals except for iron, which comes primarily from sedimentary sources [2]. These observations testify to the importance of magmatic systems in providing a flux of metals into crustal systems with consequences for hydrothermal ore formation. Understanding this process in different volcanic settings around the world and establishing the key influences on metal flux could have significant impact on exploration for ore deposits. This is one of the objectives of the NERC FAMOS (*From Arc Magmas to Ore Systems*) research programme (NE/P017371/1) of which these ion-probe analyses from part.

What limits our ability to predict metal fluxes from basaltic magmas is information on how metals partition between fluids and metals in during magma degassing. This information can be obtained either experimentally or using suites of natural samples that lie along a degassing trend. That is the approach that we have taken for a suite of olivine-hosted melt inclusions from the 1974 eruption of Fuego volcano Guatemala. This well-studied eruption of a subduction zone volcano is known to display compelling evidence for decompression-driven degassing and crystallisation [3] and for its abundant melt inclusions [4].

Olivine phenocrysts were separated and mounted in epoxy and polished down to expose melt inclusions. Melt inclusions were imaged by SEM and reflected light and analysed by EPMA . Glassy melt inclusions with diameters greater than 30 microns were then selected for analysis by SIMS. Some melt inclusions contained large co-entrapped minerals (typically Fe-Ti oxides), which were avoided during analysis. Melt inclusion compositions range from basalt to basaltic andesite. Host olivines range from Fo_{70} to Fo_{77}. Water, carbon dioxide, lithium, beryllium and boron were measured in 64 melt inclusions. Calibration was performed on basaltic glasses of known H_2O, CO_2 and trace element content. SiO_2, as measured by EPMS, was used as the internal standard.

Results

Melt inclusion H_2O contents range from less than 1 to 5.5 wt%; CO_2 ranges from the detection limit of ~50 ppm to 1500 ppm. The covariation of H_2O and CO_2 (Fig. 1a) is consistent with degassing from a melt with high initial volatile content, corresponding to a calculated saturation pressure of ~4 kbar or depth of 14 km. The degassing trajectory is less concave than would be expected for simple closed or open system degassing, indicating that some free-fluid was present in the melt at the onset of ascent, possibly coupled with mixing of magma batches sourced from different depths. Sulfur, as measured by EPMA, correlates with CO_2 (Fig. 1b) consistent with known solubility relationships in basaltic magmas [5]. The behaviour of chlorine (Fig. 1c) is more complex, showing an apparent peak at intermediate H_2O concentrations. This is consistent with a delayed onset of chlorine degassing as predicted from experimental data [5]. The increase in chlorine at high H_2O is driven by crystallisation of chlorine-free minerals without significant partitioning of chlorine into the fluid.

Future work

The next step in this research is to measure the concentrations of volatile trace metals using LA-ICP-MS. The aim is to understand how these metals are released from melts into fluids and constrain fluid-melt partition coefficients. This can be done with an arithmetical treatment of the covariation of different metals with different fluid species. The dataset is sufficiently large to make this tractable and

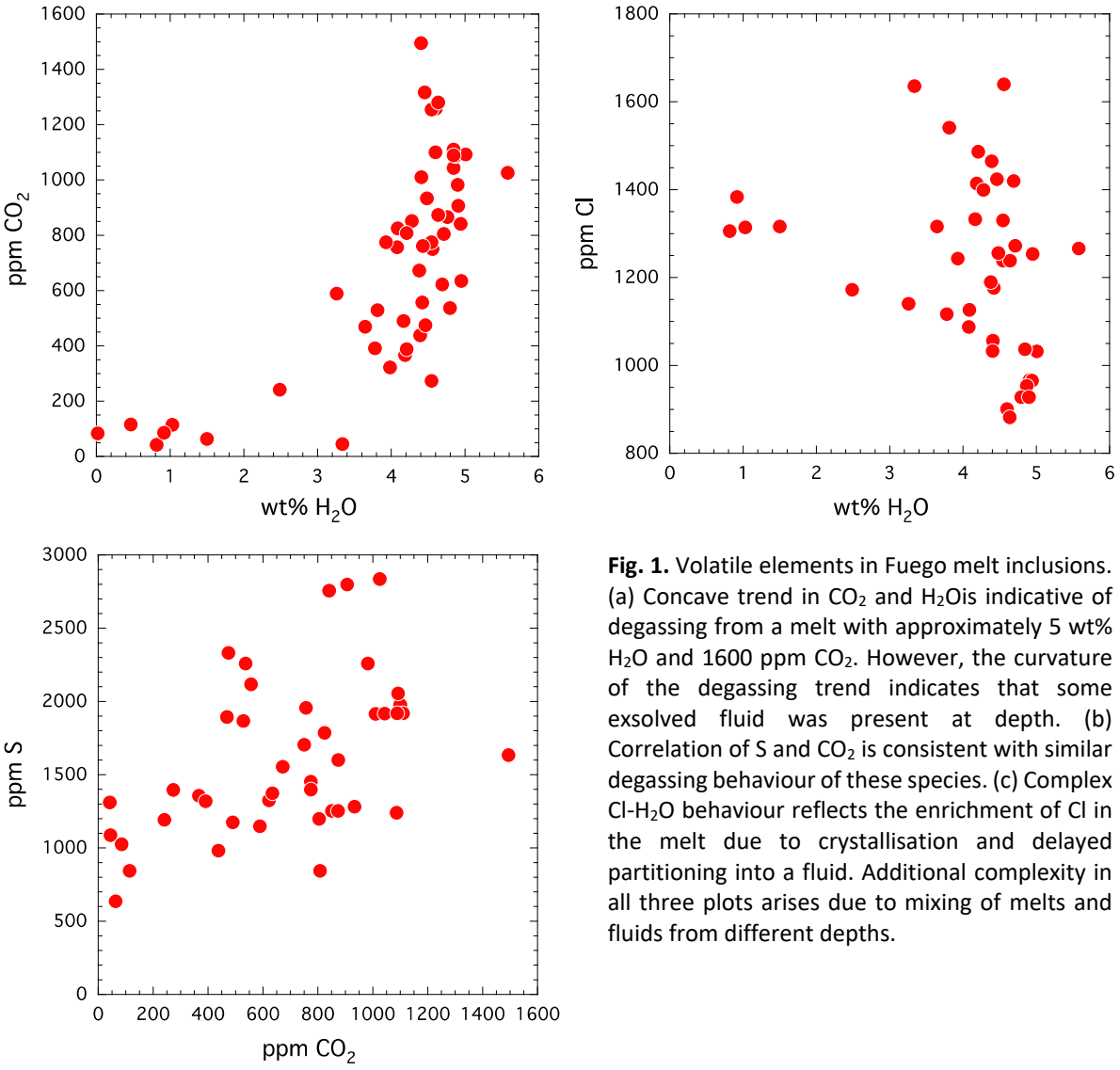

Fig. 1. Volatile elements in Fuego melt inclusions. (a) Concave trend in CO_2 and $H_2O$is indicative of degassing from a melt with approximately 5 wt% H_2O and 1600 ppm CO_2. However, the curvature of the degassing trend indicates that some exsolved fluid was present at depth. (b) Correlation of S and CO_2 is consistent with similar degassing behaviour of these species. (c) Complex Cl-H_2O behaviour reflects the enrichment of Cl in the melt due to crystallisation and delayed partitioning into a fluid. Additional complexity in all three plots arises due to mixing of melts and fluids from different depths.

take into account the effects of crystallisation, initial bubble content and changing fluid phase composition. Target metals for analysis are Cu, Zn, Pb, Sn, W, Mo, In and Sb, but we will analyse as full a suite of elements as possible, limited primarily by abundance and melt inclusion size. We will also use the Li, Be and B data acquired by SIMS to generate a comprehensive picture of how metals are released from basaltic magmas into magmatic fluids. The LA-ICP-MS analyses will be performed at the Open University in the next 2-3 months. The resulting data will be compared to measured metals fluxes from arc volcanoes [1] and more generally into an understanding of how basaltic magma inputs into arc systems can provide metals from subsequent ore formation.

References

[1] Edmonds, M., Mather, T.A. and Liu, E.J. (2018) Nature Geoscience **11**, 790-794.
[2] Hogg, O., Blundy, J. (2022). Geoscientist, Summer 2022
[3] Liu, E.J., Cashman, K.V., Miller, E., Moore, H., Edmonds, M., Kunz, B.E., Jenner, F. and Chigna, G. (2020) Journal of Volcanology and Geothermal Research **405**, 107044.
[4] Roggensack, K. (2001) Geology **29**, 911-914.
[5] Lesne, P., Kohn, S.C., Blundy, J., Witham, F., Botcharnikov, R.E. and Behrens, H. (2011) Journal of Petrology **52**, 1737-1762.

Petrological imaging of a frequently erupting arc volcano (Volcán Villarrica) using melt inclusion compositions

F. Boschetty[1], D. Ferguson[1] & P. Wieser[2]

[1]Institute of Geophysics and Tectonics, School of Earth and Environment, University of Leeds, Leeds LS2 9JT, UK
[2]Department of Earth and Planetary Science, UC Berkeley, California, USA

Motivation

Villarrica volcano is a one of Chile's most active volcanoes with over 100 eruptions since 1558 and has evidence for both vertically and laterally extensive magma storage [1]. Furthermore, while post-glacial activity at Villarrica has a large range in eruption intensity and magnitude (mafic-ignimbrite-forming to intense lava fountaining). This diversity is not reflected in the composition of erupted products, which have a limited range compared to other nearby Chilean volcanoes [1, 2]. This makes it an ideal target to study via melt inclusion (MI) compositions, which typically record a greater range of melt compositions than groundmass glasses or whole-rock, and trap volatiles which are otherwise degassed at shallow depths. We measured the volatile, trace and major element compositions of over 100 melt inclusions, and glasses from four different post-glacial eruptions (14ka–2015).

Samples and Methodology

Samples of four eruptions were collecting during a field campaign in January 2020 (Figure 1). The four eruptions sampled are: (1) The Pucón Mafic Ignimbrite (3.7ka), (2) Chaimilla Fall Deposit (3.2ka), (3) Los Nevados Parasitic Cones (<2.6 and >2.6 ka), and (4) the March 2015 Fire Fountain. Samples typically have low crystallinity (2–8%), phenocrysts comprise plagioclase, olivine and minor clinopyroxene. The CO2 of melt inclusion vapour bubbles was measured by micro-Raman spectroscopy at the Bragg Centre, University of Leeds. We then analysed, volatile and trace element composition of glassy melt inclusions in olivine, plagioclase and clinopyroxene, interstitial melt and adherent groundmass glass by SIMS. SIMS analyses were performed using the Cameca IMS 7f-Geo across two analytical sessions in October and November 2022. Boron isotopes were then measured in a third session, again using the Cameca IMS 7f-Geo, in December 2022 on a small subset of inclusions. Major element chemistry of inclusions and their hosts was subsequently measured by Electron Microprobe Analysis using a JEOL JXA8230 superprobe at the University of Leeds.

Results

Preliminary results show that MIs from each eruption occupy a broad compositional space: each eruption's MIs display distinctive degassing or dehydration paths in H_2O-CO_2 space (Figure 1), and an array of both light and heavy trace elements (Figure 2). Boron isotopes show similar values to those measured in previous studies, with no obvious trends between the different eruptions. Note that the data in shown figures are not corrected for post-entrapment modification. Measurement of the CO_2 within the vapour bubble results in high CO_2 contents (>3000 ppm) for some inclusions, highlighting the importance of the bubble as a reservoir for MI CO_2. This high CO_2 (relative to H_2O contents) may be the result of CO_2 flushing and may explain the high intensity of the 2015 eruption. Further modelling with

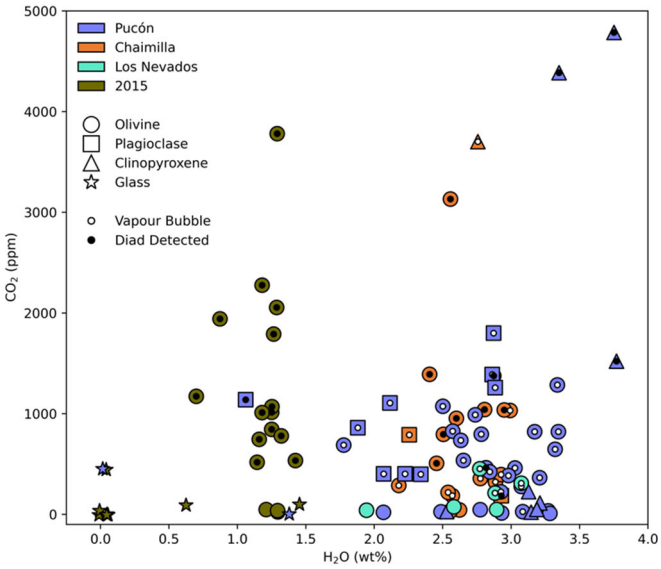

Fig. 1. H_2O-CO_2 plot showing the variation in volatile contents for Villarrica melt inclusions.

test if this is the case. Modelling of volatile contents will allow entrapment pressures to be calculated, and the vertical extent of Villarrica's magmatic system to be ascertained.

Implications

Based on these results, we hypothesise that the melts that feed eruptions at Villarrica are more diverse than their homogeneous whole-rock compositions would suggest. The variety of compositions implies complex magma storage and processing beneath Villarrica, that occurs over a range of pressures. Further modelling will test whether this is due to mixing of multiple distinct reservoirs that have evolved via homogeneous fractional crystallisation to different extents, mixed in different proportions resulting in a spread of trace-element compositions. An alternative is that boundary-layer fractionation, extensive crystallisation along the walls of reservoirs, produces a variety of liquid compositions that are then mixed back into the molten centre of a single reservoir, again producing a range of compositions [3]. Fitting of measured of melt inclusion compositions trapped during crystallisation to thermodynamic simulations will help differentiate or calculate the contribution of these two processes.

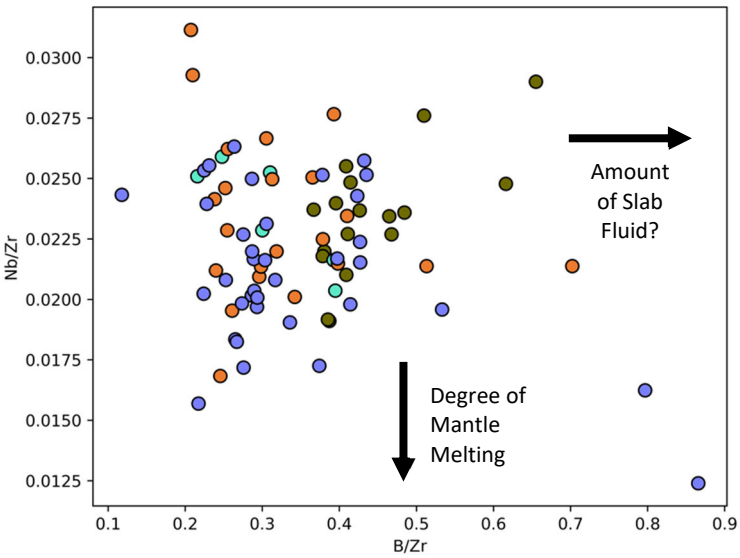

Fig. 2. Trace-element ratio plot showing the range of trace element contents of Villarrica melt inclusions. Arrows show how primary variation could affect the variation seen.

References

[1] F.O. Boschetty et al. (2022). Geochemistry, Geophysics, Geosystems. G-Cubed. 23.
[2] R. Hickey-Vargas et al. (2016). Lithos. 258, 115-132.
[3] R. Brahm et al. (2022). Journal of Petrology. 63,

The source and flux of volatiles in off-craton lithospheric mantle

J.C. Crosby & S.A. Gibson

Dept. of Earth Sciences, University of Cambridge, Downing St, Cambridge, CB2 3EQ, UK

Background

Earth's continental lithospheric mantle represents a major but poorly-understood reservoir for volatiles that are essential ingredients to build a habitable planet (H, F, Cl, Li, B, S, He, CO_2 etc). The unique ability of this reservoir to modulate the influx of volatiles from the deep Earth and their outflux to our planet's surface via volcanism makes the continental lithospheric mantle a critical component in global volatile cycles [1]. Additionally, volatile elements are fundamental to many processes in the solid Earth because they influence the temperatures and pressures of melting (e.g. H_2O & F). They also control ore-petrogenesis (Cl & Li).

Volatiles have potentially accumulated in the continental lithospheric mantle via metasomatism over billions of years and a fundamental outstanding question concerns the relative fluxes of different volatiles from recycled subducted oceanic lithosphere, or melts of primitive or depleted mantle. Because nominally-volatile-free minerals dominate the bulk of the lithospheric mantle, determining their volatile content in samples with differing styles of metasomatism is imperative to constraining the overall flux between different Earth reservoirs. Because the concentrations of volatiles within individual phases are subject to modification by sub-solidus equilibration between co-existing phases it is necessary to reconstruct bulk volatile concentrations, which requires well characterised samples. Direct analysis of volatiles in bulk samples is not an alternative due to grain boundary infiltration and crystallisation of volatile-rich host melts. SIMS analysis of individual phases in well-characterised mantle xenoliths therefore offers the most robust approach.

Methodology

Our study involved the analysis of nominally volatile-free mantle minerals (olivine and pyroxenes) using the Cameca 7f-Geo, and built on a recently completed pilot project (EIMF681/0519). The grains were separated from 10 mantle xenoliths, collected from subduction zone and circum-cratonic settings that had previously been fully-characterised for their petrography, major, trace elements and noble gases. San Carlos olivine was continually analysed multiple times per run as it is considered to have ~0 ppmw of H_2O and thereby acts as an internal reference to assess analytical drift. Cl is notoriously difficult to analyse in mantle phases because of its low concentrations and the availability of standards (Table 1). To try and overcome some of these issues, we used ALV519-4-1 (see [2]) as a Cl standard but the concentrations proved to be too low (45 ppm) to obtain reliable calibration values. We also analysed the same grains of clinopyroxene by Li by LA-ICP-MS at the University of Cambridge to establish the accuracy of this rapid analysis technique in future studies.

Table 1. Standards used for SIMS calibration during analysis of nominally volatile free mantle phases.

Standard	H2O (ppmw)	Li (ppm)	B (ppm)	F (ppm)	P (ppm)	Cl (ppm)
ALV-519-4-1	1700	3.6	0.5	95	302	
OPX-KH03-4-3	216			25	10.6	
OPX-116610-3	128			17.4	0.5	
CPX-KH03-4-1	427			64.8		
CPX-SC-J1-1	62			26	30.9	
CPX-SMC31139-1	5			0.5		
ST8.1.A92-2						2026.1

Results

The new set of SIMS analyses significantly expands the global database for volatiles in mantle phases (especially for F, Cl, Li, and B). Importantly, the dataset is internally consistent and allows a more robust statistical analysis than was previously possible of what controls the concentration and partitioning of

these volatiles between mantle phases [3, 4, 5]. Although Cl contents were very low in mineral separates from most samples, we observed an increase of bulk xenolith F/Cl with ^{3}He and CO_2 contents.

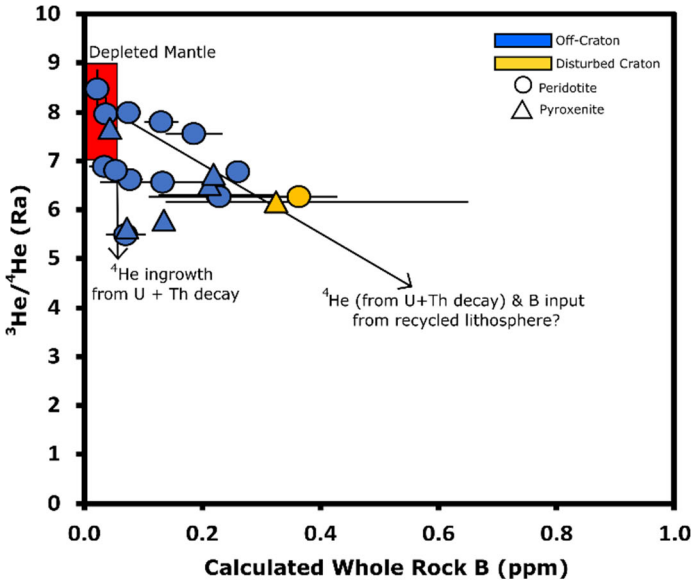

Fig. 1. Calculated whole-rock B (ppm) compared to calculated whole-rock ^{3}He/^{4}He (Ra). Horizontal lines show uncertainties in whole-rock B contents.

Our study has greatly increased the amount of available data for B in mantle peridotites. The highest whole-rock B contents were observed in mantle peridotites associated with subduction related metasomatism. Interestingly, B contents do not always correlate with F/Cl, which suggests that metasomatic fluids may be being released as different phases become unstable (i.e. at variable depths) in the down-going slab. A novel finding from our study is that there appears to be a negative correlation between B and ^{3}He/^{4}He in some of our samples (Figure 1). This suggests a metasomatic input from recycled oceanic lithosphere and offers a further opportunity for using B in nominally volatile-free phases as a tracer of volatile source regions.

References

[1] S. A. Gibson, D. McKenzie, Earth and Planetary Science Letters **602**, 117946 (2023).

[2] B. M. Urann et al., Contributions to Mineralogy and Petrology **172**, 51 (2017).

[3] S. A. Gibson, E. Rooks, J. A. Day, C. M. Petrone, P. T. Leat, Geochimica et Cosmochimica Acta. **275** 140–162 (2020).

[4] J. C. Crosby, The nature and co-behaviour of volatile and non-volatile elements in the sub-continental lithospheric mantle (PhD thesis, University of Cambridge, UK, 2021, 200pp).

[5] J. C. Crosby, S. A. Gibson, F. M. Stuart, T. R. Riley, L. Di'Nicola, (2021). https://doi.org/10.7185/gold2021.7412

Determining hydrogen plagioclase-melt partition coefficients in silicic melts

K. Cutler[1], M. Cassidy[2] & J. Blundy[1]

[1]Department of Earth Sciences, University of Oxford, South Parks Road, Oxford, OX1 3AN, UK

[2]School of Geography, Earth and Environmental Sciences, University of Birmingham, Edgbaston, Birmingham, B15 2TT, UK

Introduction and Background

Water is the most abundant volatile species in silicate melts, exerting important controls on the physical and chemical properties of magma, and on eruption style. Direct analysis of volatile concentrations in nominally anhydrous minerals (NAMs) represents a promising alternative to constrain H_2O contents alongside existing methods (i.e. melt inclusions, mineral-melt equilibria). NAMs can accommodate trace concentrations of hydrogen (i.e. hydroxyl, OH) within their crystal structures, which can serve as a proxy for determining magmatic water concentrations if a partition coefficient between the hydrogen in the mineral of interest and melt is known at the relevant conditions. Using plagioclase as a hygrometer has great potential due to the slower H^+ diffusivity of plagioclase compared to other NAMs [1]. However, not much work has explored hydrogen plagioclase-melt partitioning, with current experimental constraints limited to mafic melts [2,3,4]. Here we look at examining hydrogen plagioclase-melt partitioning under silicic conditions to test a wider range of variables (e.g., H_2O content, temperature, SiO_2 content, degree of polymerisation, mineral chemistry, pressure) that could influence partitioning behaviour.

Preliminary Results

We have carried out hydrogen plagioclase-melt partitioning experiments in cold seal pressure vessels, using a synthetic haplogranite as starting material. Preliminary data reaffirms that melt water content is the dominant factor controlling hydrogen partitioning, with higher partition coefficients ($D_H^{plag/melt}$ > 0.003) resulting from changes in water speciation (Fig. 1; <1 wt.% OH and <0.5 wt.% molecular water (5)). No plagioclase standards were available during the pilot study, so a hydrous glass calibration curve was used to process the hydrogen analyses. In addition, major problems were encountered during the pilot study (e.g., high relief of vesicular experimental samples and small crystal sizes), which made it difficult to pick out clear analytical points using the SIMS camera. We have made changes to experimental and polishing procedures to overcome these issues for future analysis. We plan to analyse more experiments to further investigate other factors affecting H partitioning. Analyses of plagioclase phenocrysts from the Plinian phase of the May 1980 Mount St Helens eruption will also help to evaluate the new hygrometer by comparing the H_2O concentrations to estimates from melt inclusions, experiments, and plagioclase-liquid/liquid-based hygrometers.

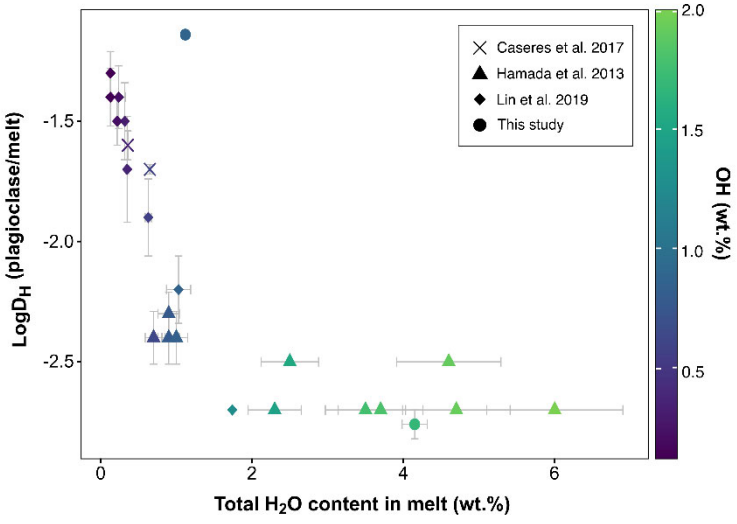

Fig. 1. Experimental plagioclase-melt partition coefficients vs. total water content in the melt. Data points coloured according to hydroxyl (OH) content, calculated from VolatileCalc [5].

References

[1] Johnson E.A. and Rossman G.R. (2013) American Mineralogist 98(10), 1779-1787
[2] Hamada M. et al. (2013) Earth and Planetary Science Letters 365, 253-262
[3] Caseres J.R. et al. (2017) 48th Annual Lunar and Planetary Science Conference 1964, 2303
[4] Lin Y.H. et al. (2019) Geochemical Perspectives Letters 10, 14-19
[5] Newman S. and Lowenstern J.B. (2002) Computers & Geosciences 28(5), 597-604

Multiple elemental and isotopic constraints on individual melt inclusions?

D. Ferguson, F. Boschetty, J. Harvey & I. Savov

Institute of Geophysics and Tectonics, School of Earth and Environment, University of Leeds, Leeds LS2 9JT, UK

Motivation

Subduction zones are the primary tectonic environment where elements are cycled between the Earth's solid interior and its outer fluid envelopes. These geochemical cycles, such as the deep carbon cycle, exert a fundamental control on Earth's climate and habitability over geological time. However, quantifying outward elemental fluxes at subduction margins is challenging due to difficulties in constraining both the inventory of volatile elements in subduction zone magmas and the origins of the magmas, which can be derived from a variety of source components. Micro-analysis of melt inclusions (MIs) has provided a powerful tool to constrain magmatic volatiles, as the included melts are protected from low pressure volatile loss via degassing. Constraining the origins of melts, with respect to the relative contributions of source components in magma creation, such as the subducted slab versus sub-arc mantle wedge, is typically achieved using whole-rock isotopic data (e.g., $^{87}Sr/^{86}Sr$). There is therefore a dichotomy between the spatial scales of analysis associated with each of these techniques, i.e. microanalysis of volatiles versus whole-rock isotopic analysis. The overarching aim of our project, which this pilot proposal contributes towards via measurement of boron isotopes, is to collect a proof-of-concept dataset comprising volatile, trace, and major element and B, Sr, and Nd isotopic data on individual MIs.

Samples and Aims

Our samples are large melt inclusions (>100 microns in diameter; Fig 1) from Villarrica volcano in S. Chile. These represent subset of a suite of MIs that have been previously analysed via another IMF proposal for volatile (C and H) and non-volatile trace elements (Boschetty et al. report). The aim of our pilot proposal is to add B isotopic data to the suite of analyses we are collecting on these inclusions. B is a volatile element that is very depleted in the mantle but very enriched in the subducted slab. B data can therefore provide important constraints on the transfer of materials from the slab to the region of magma generation in the mantle beneath volcanic arcs [1]. In situ B isotopic data for MIs in which we have also measured H_2O and CO_2 contents (the latter by both SIMS and Raman microscopy on the MI vapour phase) has the potential to provide important new constraints on the precise origin of these volatiles within the sub-arc environment, which, unlike B, may not necessarily originate from the subducted slab [2].

Results and ongoing work

Boron isotopes and concentrations were measured in 15 MIs using the Cameca IMS 7f-Geo in December 2022. The B data (Fig 2) shows a range of $\delta^{11}B$ from -7 to 3‰., with variations above the 2-sigma uncertainty. These are elevated relative to the MORB-mantle and are similar to, but extend to lower values than, previous δ11B analyses for Villarrica [3]. The lowest $\delta^{11}B$ are approaching those of MORB (-7‰) and our data implies variable, and in some cases low, amounts of slab input. Given the observed variations we are hopeful of finding resolvable differences in the radiogenic isotopic compositions of the MIs that correlate with $\delta^{11}B$. We are in process of extracting these inclusions from their host crystal for isotopic analysis via Thermal Ionization Mass Spectrometry (TIMS).

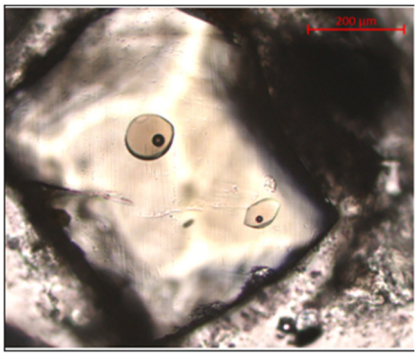

Fig. 2. Olivine crystal with large (>100 micron) basaltic melt inclusion with internal vapor bubble.

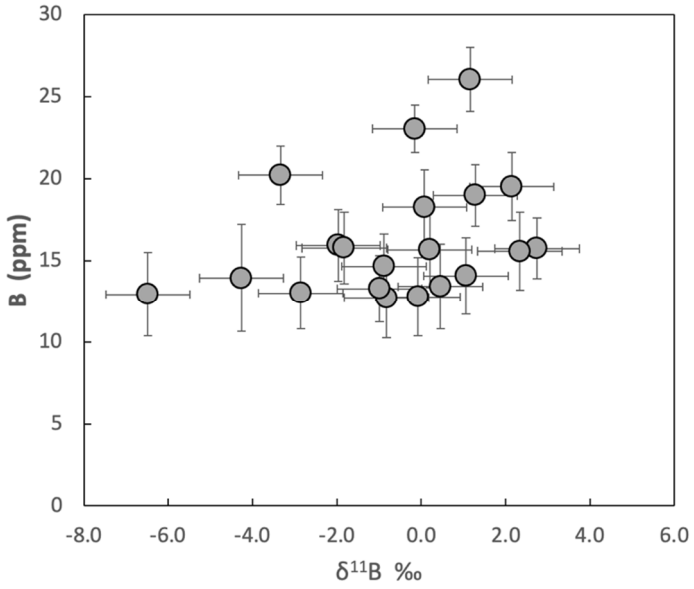

Fig. 3. Boron concentrations and isotopic data for melt inclusions from Villarrica.

References

[1] De Hoog, J.C.M. and I. Savov (2018) In 'Boron Isotopes – The Fifth Element' pp. 217-247.
[2] E. Mason et al (2017) Science 357, 290-294
[3] S. Turner et al. Unpublished IMF data

The suitability of synthesised glass monoliths for use in lithium and boron isotope tracer dissolution studies

T.L. Goût & I. Farnan

Dept. of Earth Sciences, University of Cambridge, Cambridge CB2 3EQ, UK

Background and rationale

The internationally recognised solution for high-level nuclear waste that arises as a by-product from the reprocessing of spent nuclear fuel is vitrification, producing a glassy waste-form destined for permanent geological disposal. However, as a metastable phase, the weathering of these glasses can result in anthropogenic radionuclide release. The safety case for the geological disposal of waste rests on establishing models capable of predicting over the facility's lifespan (1 Ma) (1) the kinetics of radionuclide release during glass-groundwater interactions and (2) the subsequent diffusive or advective transport of these radionuclides through the engineered disposal facility barriers and the geosphere. The former relies upon mechanistic weathering models alongside maximum release rates (source-terms), but the mechanisms underpinning glass weathering as a function of glass composition and environment remain highly conflicted. Research presented in the literature is highly reliant upon analysis of weathered samples *ex-situ*, with the associated mechanisms subsequently being inferred from altered surface layer structures, glass hydration and secondary phase precipitates.

Previous works have shown that measuring the δ^7Li values of the resulting glass waters presents a promising means for quantitatively tracing the mechanisms underpinning the observed kinetics *in-situ*: δ^7Li values measured throughout a weathering experiment affords the resolution of the contributions of congruent dissolution (hydrolysis of the glass network), incongruent dissolution (diffusive transport) and precipitation (predominantly clays) to dissolution kinetics through a mass balance model [1]. However, not all nuclear waste glasses contain Li, and B is instead often used as a tracer of dissolution kinetics. The use of δ^{11}B values as similar mechanistic tracers to δ^7Li values is complicated through (1) B occupying a mixture of trigonal and tetrahedral sites in most borosilicate glasses and (2) B being present predominantly as trigonal boric acid ($B(OH)_3$) or a tetrahedral borate anion ($[B(OH)_4]^-$) in dilute aqueous solutions (depending upon pH) [2]. The former is sensitive to thermal history and is the focus of this work. It was postulated that the sensitivity of the trigonal to tetrahedral B site ratio to cooling rates can produce structural heterogeneity where the outer 'skin' of an as-cast glass monolith (coupon) has a significantly higher cooling rate than its core.

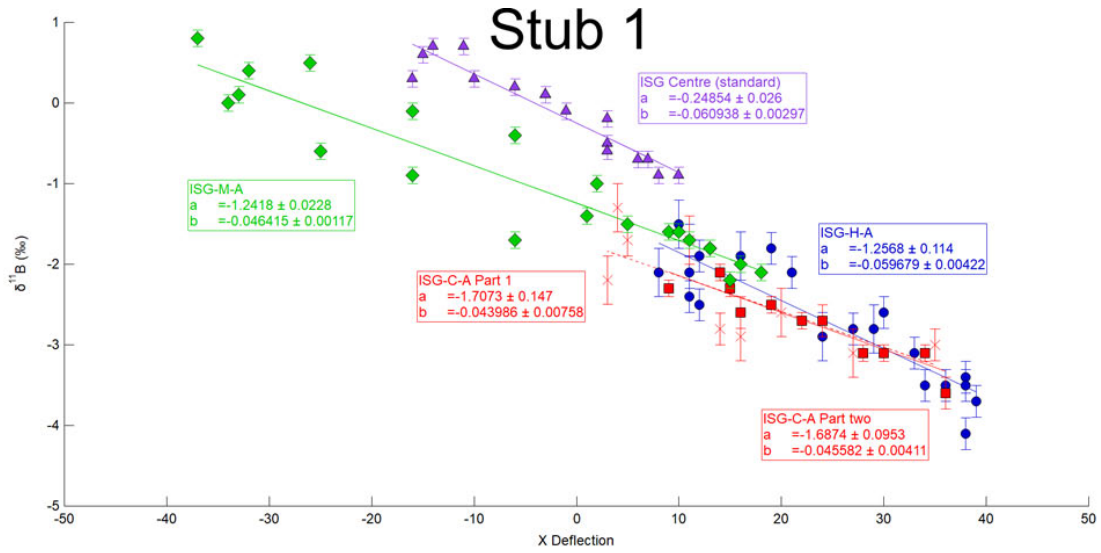

Fig. 4. Measured δ^{11}B values plotted against X-deflection. Points represent the X-deflections for each individual measurement, whilst lines represent simple linear regressions (coefficients and standard errors given in boxes).

Given an equilibrium fractionation factor describing the distribution of $\delta^{11}B$ values across the trigonal and tetrahedral B units as a function of temperature, this suggests that the $\delta^{11}B$ value associated with each unit would vary as a function of distance from the glass core. Ultimately, noting evidence for the preferential hydrolysis of trigonal over tetrahedral B units [3], this would result in a changing $\delta^{11}B$ value from the glass with time during weathering even in the absence of changes in the underpinning mechanisms. The objectives of this work are therefore to investigate the potential effect glass thermal history may have on isotopic homogeneity ($\delta^{7}Li$ and $\delta^{11}B$) of glasses of dimensions typically synthesised for laboratory experiments and subsequently to define limits in terms of cooling rates for this homogeneity.

Approach and preliminary results

For the ion micro-probe analysis, 12 glasses were synthesised as cylinders of different compositions and thermal histories based upon the well-studied glass International Simple Glass (ISG), ISG with Li additions, and ISG with Li and Mg additions. Slices were then cut from the centre of each cylinder and were then cut into quarters for analysis using the Cameca IMS 7f-Geo. Samples were analysed for $\delta^{11}B$ and $\delta^{7}Li$ (where the sample contained Li) along each edge of the each glass specimen, using a specimen prepared from the centre of a block of ISG as the in-house standard for drift corrections. This block of ISG was prepared externally (MoSci Corporation, US) and had been previously characterised across a number of studies. Note that ISG contains no Li and has not been previously characterised for its $\delta^{11}B$ values.

Notably, a significant negative correlation was observed between the measured $\delta^{11}B$ value and the X-deflection (Figure 1). This was confirmed through analysing the samples twice at rotations of 0 and 90° and through analysing a set of secondary standards (GB4, B6, GSD, UTR1 and ARM-1,-2 and -3) and a sample of Duran glassware. No correlation was observed for the Y-deflection, such that the samples could be corrected through a simple linear regression. Where such corrections were performed, propagated uncertainties included those associated with the regression.

The results corrected for X-deflection biases at both 0 and 90° were typically consistent with the $\delta^{11}B$ values across all samples being homogeneous, with some single-point outliers (Figure 2). Whilst Li potentially exhibited some $\delta^{7}Li$ value trends across some samples, the absence of an in-house standard for reliable drift correction measurements introduced significant uncertainty into these trends. These results were therefore consistent with the absence of a measurable thermal effect for the $\delta^{11}B$ values at the scale and thermal histories investigated, thereby validating the use of these monoliths in B isotope tracer weathering experiments. Current work is in progress to define theoretical lower limits for the cooling rate gradients required to cause measurable heterogeneity as a function of glass composition and monolith geometry.

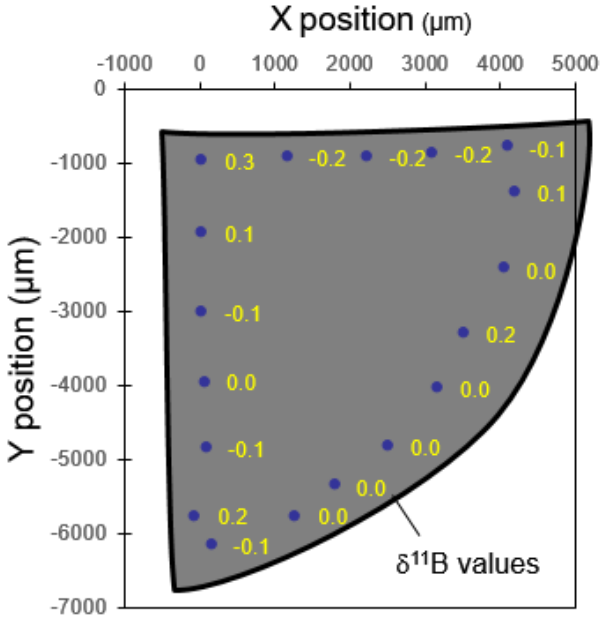

Fig. 2. Corrected $\delta^{11}B$ values for a heat-treated coupon segment (LiMgISG-C).

References

[1] T.L. Goût et al. (2021) Geochimica et Cosmochimica Acta, 313, 133–154.
[2] H. Kakihana et al. (1977) Bulletin of the Chemical Society of Japan, 50, 158–163.
[3] H. Aréna et al. (2019) Npj Materials Degradation, 3 1–11.

Fluid-mobile elements in garnet as recorders of fluid pulses

R. Halama[1], M. Konrad-Schmolke[2] & J. De Hoog[3]

[1]School of Geography, Geology and the Environment, Keele University, Keele, ST5 5BG, UK
[2]Department of Earth Sciences, University of Gothenburg, Gothenburg, Sweden
[3]School of GeoSciences, University of Edinburgh, Edinburgh EH9 3JW, UK

Introduction

Garnet is a useful mineral in recording geochemical changes during growth. In this pilot study, we have analyzed H_2O and fluid-mobile element (FME; F, Cl, Li and B) concentrations in a garnet crystal in a blueschist from Hispaniola to assess whether changes in rare earth element (REE) concentrations are associated with changes in fluid chemistry. The garnet shows smooth core-to-rim major element zoning typical for growth during high pressure/low temperature subduction zone metamorphism, whereas the REE zoning patterns are more complex and include rhythmic fluctuations [1]. Concentrations of H_2O and FME concentrations were measured in gold-coated thin sections using the Cameca 7f-GEO secondary ion mass spectrometer at the Edinburgh Ion Microprobe Facility.

Results

Measurements were carried out along a core-to-rim profile across a zone with several peaks in REE contents (Fig. 1). Water and the FMEs analysed (F, Cl, Li and B) yield quantifiable concentrations. Compositional variations in the FME contents are small and do not correlate with the REE fluctuations (Fig. 1). Water contents vary from 50 to 80 µg/g and show a slight decrease from core to rim, similar to F (8-22 µg/g). Lithium and B concentrations increase slightly from 1 to 2 and 30 to 70 µg/g, respectively. Chlorine concentrations are constant between15 and 25 µg/g throughout the profile.

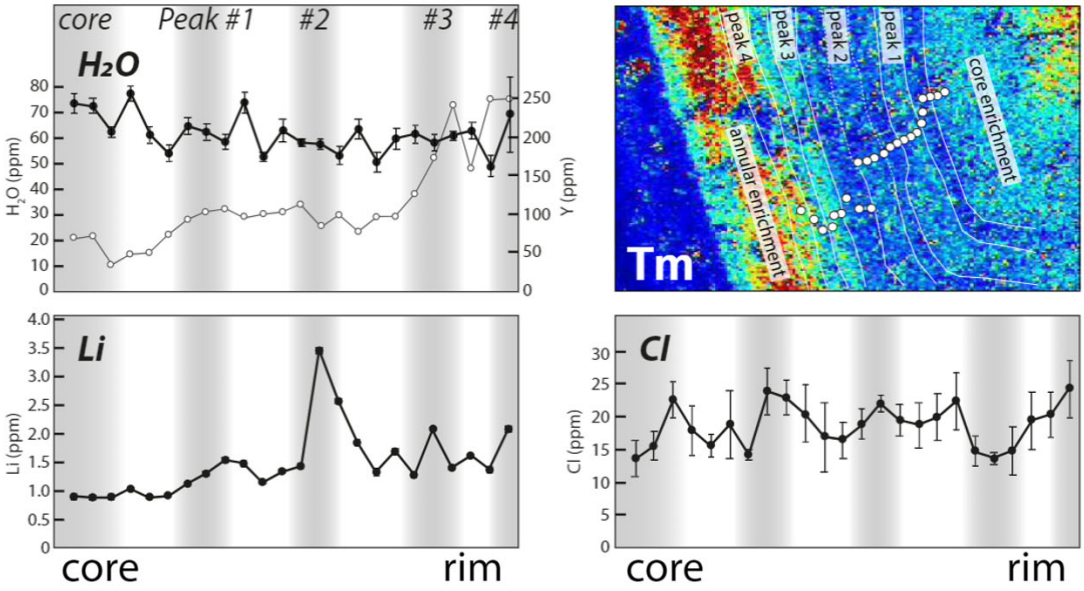

Fig. 1. Results of water, Li and Cl measurements in garnet. Spot positions are shown on the Tm map on the upper right panel. Grey bars in the diagrams show the approximate positions of the REE peaks.

Interpretation

The relatively water contents suggest that an aqueous fluid was always present during garnet growth. The small variations in FME contents, which are unsystematic with respect to REE fluctuations, point to no significant influence of changing fluid chemistry or salinity on REE incorporation into the garnet. Instead, REE fluctuations result from changing element transport properties of the rock that can be explained by pulse-like fluid fluxes [1].

References

[1] M. Konrad-Schmolke et al. (2022) Journal of Metamorphic Petrology, DOI: 10.1111/jmg.12703

The fate of nitrogen in volcanic arcs

R. Halama[1], R. Gertisser[1], A. Iveson[2] & J. De Hoog[3]

[1]School of Geography, Geology and the Environment, Keele University, Keele ST5 5BG, UK
[2]Department of Earth Sciences, Durham University, Durham DH1 3LE
[3]School of GeoSciences, University of Edinburgh, Edinburgh EH9 3JW, UK

Introduction

The aim of this pilot study was to determine the feasibility of nitrogen (N) concentration measurements in mafic melt inclusions as a proof-of-concept dataset. To obtain data on N concentrations in melt inclusions of primitive arc magmas is an important contribution to better quantify the N outflux in volcanic arcs and the transfer of N from the subducting slab into the arc magma sources. These data will ultimately provide constraints on the evolution of the Earth's unique N-rich atmosphere through geologic time [1].

Results

Measurements were undertaken using the same analytical setup as used for routine CO_2 analysis at the IMF using the Cameca 7f-Geo ion microprobe. Nitrogen background signals were low (< 1 ppm in N-free pyroxene). We obtained N concentrations in the range 1-28 ppm for olivine-hosted, non-homogenised melt inclusions from 3 volcanic centres in Kamchatka. These concentrations are similar to published values [2] and demonstrate that N in silicate glasses with concentrations as low as c. 1 ppm can be successfully measured.

Interpretation

Nitrogen contents show no systematic relationship to CO_2 contents (Fig. 1), suggesting that N was at least partly sequestered into fluid bubbles, as proposed previously [2]. There is also no systematic relationship with B contents, which show clear differences depending on the volcanic complex sampled. Nevertheless, the results provide a proof of concept with respect to future applications and analysis of rehomogenised melt inclusions, in which N concentrations are expected to be 2-5 times higher [2].

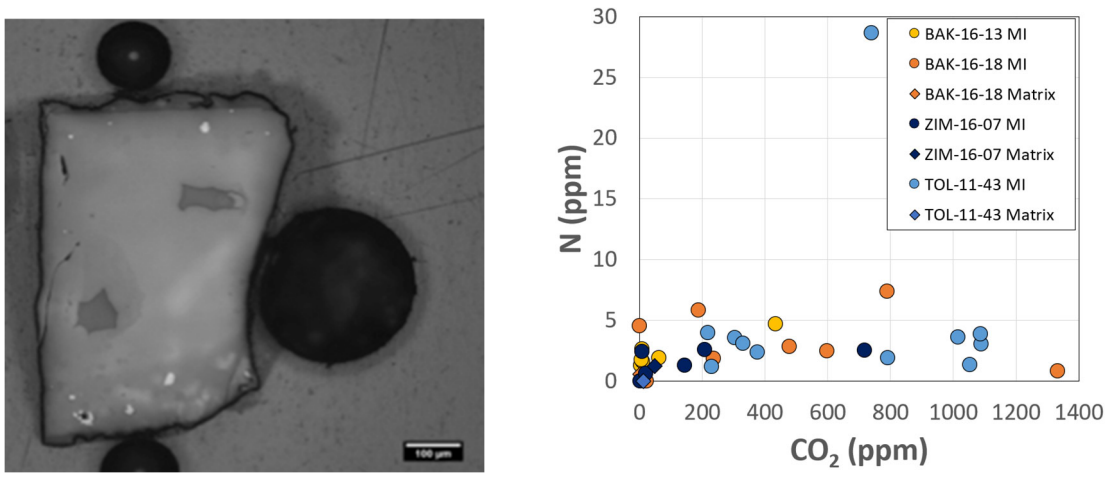

Fig. 1. Left: Olivine with melt inclusions from Bakening volcano, Kamchatka. Size of inclusion in the lower left is 80 µm. Right: N and CO_2 concentrations measured in melt inclusions (MI) and in matrix glass; BAK = Bakening, ZIM = Zimina, TOL = Tolbachik.

References

[1] R. Halama and G. Bebout (2021) Space Science Reviews **217**, 45.
[2] E. Füri et al. (2021) Chemical Geology **582**, 120456.

Boron isotope disequilibrium between tourmaline and phengite during ultra-high pressure metasomatism and metamorphism

B. J. R. Harris[1], J. C. M. De Hoog[1], R. Halama[2], H-P. Schertl[3] & Y-X. Chen[4]

[1]School of GeoSciences, University of Edinburgh, Edinburgh EH9 3JW, UK
[2]School of Geography and Geosciences, University of St. Andrews, St. Andrews KY16 9AL, UK
[3]Institut für Geologie, Mineralogie & Geophysik, Ruhr-Universität Bochum, Germany
[4]University of Science and Technology of China, Hefei, China

Introduction

Boron is a fluid-mobile element with two stable isotopes that are strongly fractionated between aqueous fluids and many common mineral phases. B isotopes are useful for tracing fluid-rock interaction and fluid sources in subduction zones due to the large variations in B isotope composition of different subducted lithologies (e.g. [1, 2]). The Dora Maira Massif in the Western Alps (Fig. 1) exposes ultra-high pressure (UHP) continental rocks which have experienced subduction to >100 km depth. Lenses of garnet-phengite whiteschist are the primary recorders of UHP metamorphism, and are interpreted as metasomatic alteration products of the host metagranite. There is outstanding debate as to the source of the metasomatic fluids, although most studies point towards fluids derived from dehydration reactions in the subducting slab during Alpine metamorphism [e.g. 3, 4].

To resolve fluid sources we previously measured B isotopes and FME in phengite from Dora Maira [IMF699/1119]. The data obtained suggest that sediment-derived fluids interacting with dehydrating serpentinites may have been involved in whiteschist metasomatism. Our findings differ somewhat from the conclusions of a recently published dataset of B isotope data for tourmaline in Dora Maira whiteschist, which suggested that the whiteschist metasomatic fluid was sourced from dehydration of deep mantle wedge serpentinites [5]. Comparing the B isotope values for tourmaline (-9.4 to -0.1 ‰, mean = -6.3 ± 2.3 ‰, n=68) [19] with our values for phengite (-15.6 to -5.7 ‰, mean = -10.6 ± 2.6 ‰, n=16) [IMF699/1119] suggests a B isotope fractionation $\Delta^{11}B_{phengite\text{-}tourmaline}$ of only -4 ‰. This is smaller than several experimental, theoretical and natural estimates of phengite-tourmaline isotope fractionation, which predict a value of around -10 ‰ [e.g. 6]. However, given the significant variation (>10 ‰) in phengite and tourmaline B isotope compositions both within and between various whiteschist samples, it is difficult to interpret the significance of this discrepancy. This discrepancy results in different estimates for the composition of the fluid, which results in different contributions of various fluid sources.

Project objectives

We set out to test the hypothesis that phengite and tourmaline are in isotopic equilibrium and were formed during the same metasomatic event. The apparent B isotope disequilibrium between previously measured tourmaline and phengite would then reflect a heterogeneous fluid in space or time. To achieve this we acquired the tourmaline-bearing samples analysed by Xiong et al. [5] and analysed B isotopes in tourmaline and coexisting phengite by SIMS.

Results and discussion

The difference in boron isotope composition between coexisting phengite and tourmaline is small but somewhat variable, with mean $\Delta^{11}B_{phe\text{-}tur}$ of -1.6, -2.6 and -5.0 ‰ in three separate samples. The difference between tourmaline rims and immediately adjacent phengite grains ranges from -3.7 to -1.1 ‰ (one outlier at +4.3 ‰). These values differ significantly from predicted equilibrium fractionation between tourmaline and mica ($\Delta^{11}B_{phe\text{-}tur}$ = -12.3 to -8.2 ‰) [6] at the temperatures where metasomatism has been interpreted to have taken place. There are also systematic differences in B concentration and isotopic composition of phengite in samples with and without tourmaline, even in samples from the same locality (Fig. 1). Phengite in tourmaline-bearing samples has a mean boron isotope composition of -6.0 ± 1.0 ‰ (n=26) with 198 ± 20 µg/g B. Phengite in non-tourmaline bearing

samples has a consistently lighter boron isotope composition (-10.6 ± 1.2 ‰, n=25) and contains less B (171 ± 14 µg/g). Interestingly, phengite in non-tourmaline bearing samples does in fact have B isotope values which would be in equilibrium with the tourmaline at the conditions of tourmaline growth, suggesting that both could have equilibrated with the same fluid. Phengite from tourmaline-bearing samples is therefore anomalous.

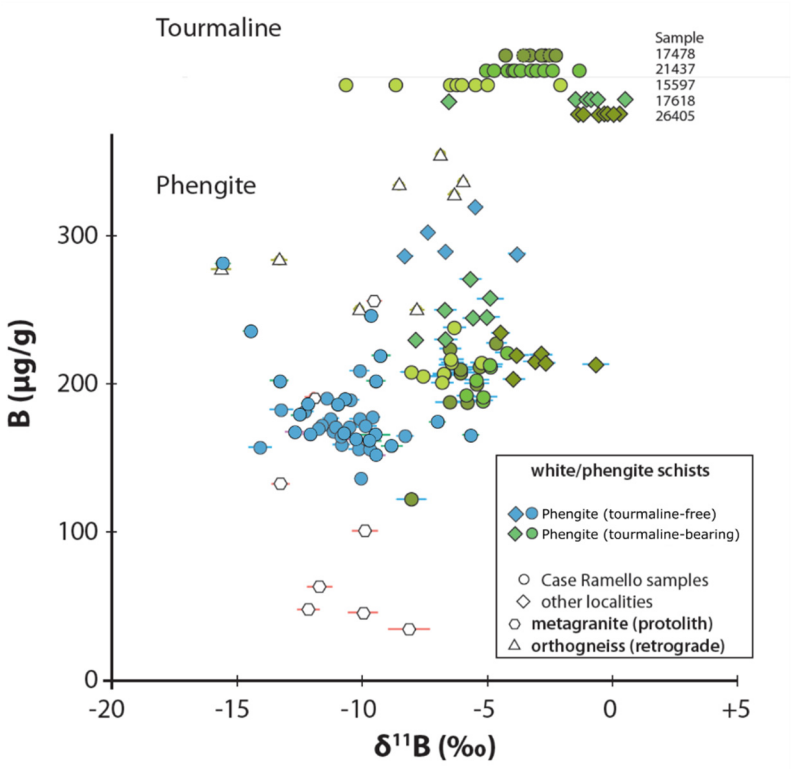

Fig. 1. Boron isotopes and B concentrations for coexisting phengite and tourmaline in metasomatic whiteschists and phengite schists, as well as the metagranite and orthogneiss country rocks. Metasomatic samples are divided into tourmaline-bearing (green) and tourmaline-free (blue), and separated by locality (circle and diamond shapes). Phengite in tourmaline-bearing samples displays consistently higher B concentrations and heavier B isotopes than phengite in tourmaline-free samples.

Error bars are 1s and smaller than symbols size if not drawn.

A possible scenario is that isotopically heavy boron was added to phengite after the growth of tourmaline. The obvious reservoir of heavy boron is the tourmaline itself. Mass balance calculations show that for every 1 wt% of phengite in the rock, 0.006 wt% of tourmaline must be dissolved and this boron incorporated into phengite in order to produce the phengite composition observed in tourmaline-bearing samples. For a whiteschist containing 40% phengite this means that 0.25% tourmaline must be dissolved. Given the significant (5%) tourmaline modes in most tourmaline-bearing samples this is not unreasonable. If ^{11}B was preferentially leached from tourmaline, as expected from tourmaline-fluid boron isotope fractionation ($\Delta^{11}B_{tur\text{-}fluid}$ =-0.5 ‰), then the amount of dissolution required would be even smaller. This would also explain the presence of thin, isotopically light rims we observed on some tourmaline grains. It remains unclear how B isotopes would have homogenised in phengite without re-establishing equilibrium with tourmaline, but perhaps there is a kinetic control as B diffusion in phengite is likely to be much faster than in tourmaline, in which it is a structural component. In any case, caution should be applied interpreting phengite from tourmaline-bearing samples as representing equilibrium B isotope fractionation.

References

[1] S Angiboust et al. (2014) J Petrol 55, 883-916
[2] M Konrad-Schmolke & R Halama (2014) Lithos 208-209, 393-414
[3] YX Chen et al. (2016) Earth Planet Sci Lett 456, 157-167
[4] S Ferrando et al. (2009) J Metamorph Geol 27, 739-756
[5] J-W Xiong et al (2022) Geochim Cosmochim Acta 320, 122-142
[6] P Kowalski et al (2013) Geochim Cosmochim Acta 101, 285-301

Variation of nitrogen concentrations and mineral partitioning with metamorphic grade in subducted oceanic basalts

B. J. R. Harris[1], J. C. M. De Hoog[1] & R. Halama[2]

[1]School of GeoSciences, University of Edinburgh, Edinburgh EH9 3JW, UK

[2]School of Geography and Geosciences, University of St. Andrews, St. Andrews KY16 9AL, UK

Introduction

The Earth's atmosphere is presently composed of 78% nitrogen and is essential for the habitability of the planet. There is considerable debate over the long term evolution of the mass of N in the atmosphere [1] and it is therefore necessary to quantify the flux of N between the surface and the mantle. Subduction zones are the primary locations for return of N from the surface to the mantle but estimates of this flux are uncertain. Studies in sediments have demonstrated retention of N to depths of at least 60-70 km in cold subduction zone settings, but significant N loss in warm subduction zones. Further studies are required to investigate the processes controlling this behaviour, including its mineralogical controls, in mafic and ultramafic sections of the subducting lithosphere. This will enable more accurate modelling of N recycling in different subduction zones and through time.

Nitrogen exists most commonly as ammonium (NH4+) in silicate minerals, substituting for K due to its similar ionic radius. White mica (predominantly phengite) is the main K-bearing phase at HP conditions in a range of bulk compositions and is critical in controlling the N budget of deeply subducted rocks [2]. The residency of N in K-poor mafic (e.g., unaltered MORB) and ultramafic sections of the oceanic crust is less well constrained, since phengite modes are often low (<5% to absent).

A previous project (IMF 709/0520, [3]) demonstrated the utility of in situ analyses of N in phengite and other minerals by ion microprobe. We confirmed that white micas (phengite and paragonite) are a significant host for N in a range of subduction-related lithologies. We demonstrated N loss during metamorphic fluid-rock interaction and used these data to place constraints on the phengite-fluid partition coefficient for N by comparing the behaviour of N to other fluid-mobile elements such as B and Li. Chlorite was also found to contain N in one sample (10-83 ppm N in chlorite, coexisting with 108-270 ppm N in phengite). Chlorite has not been previously considered as a host for N but is common in subducted rocks at lower metamorphic grades, and therefore could potentially be important for subduction zone N budgets.

The objectives of this study were 1) to systematically explore N concentrations, and its distribution between mineral phases, in samples from different metamorphic facies (greenschist, blueschist, eclogite) representing different stages of subduction dehydration. 2) Compare the behaviour of N to other fluid-mobile elements to understand how N is lost during dehydration. 3) Compare the behaviour of N in K-rich (phengite-bearing) versus K-poor (phengite-absent) samples.

Samples

We analysed 16 samples comprising greenschists, blueschists and eclogites from a range of localities including the Western Alps, Japan, Syros and the Dominican Republic. The samples were selected to represent the subducted equivalents of MORB-type basalts with varying degrees of seafloor alteration, reflected in their K_2O concentrations, ranging from <0.1 – 1.8 wt% (fresh MORB = 0.14 ± 0.01 wt%).

Results and discussion

The presence of white mica in a sample depends largely on its bulk K_2O content. Bulk K_2O > 0.4 wt% results in the presence of phengite. Samples with lower K_2O contain either paragonite, or no white mica at all. White micas contain the highest concentrations of nitrogen in all samples where they are present. In greenschists the N concentrations of phengite and coexisting actinolite and chlorite overlap significantly (Fig. 1), although phengite still has the highest mean N concentration. In blueschists and eclogites, the difference in N concentration between white micas and other phases is more

pronounced, suggesting that there are changes in inter-mineral N partitioning with metamorphic grade.

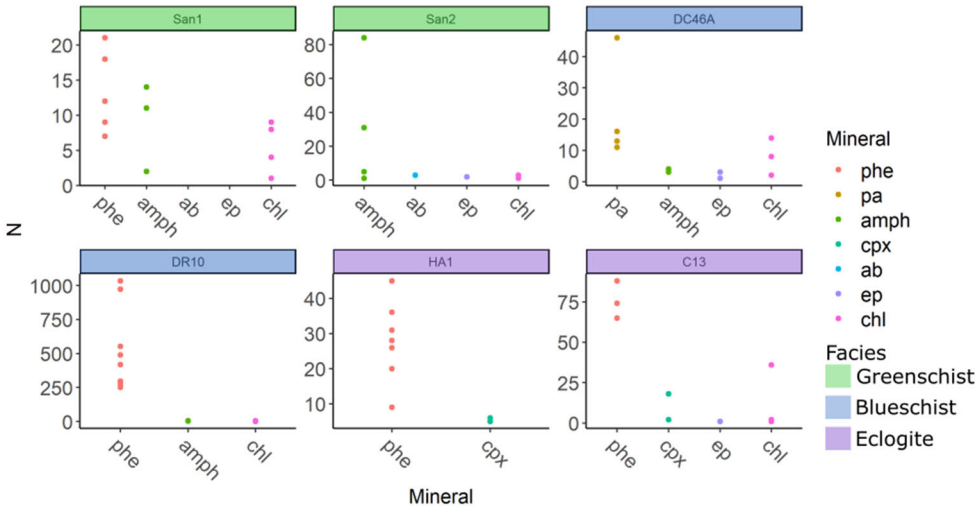

Fig. 1. Nitrogen concentrations in different minerals in selected samples from a range of metamorphic facies.

Some previous studies have suggested that NH_4^+ behaves similarly to Rb^+, since they have the same charge and a similar ionic radius [e.g. 4]. In our samples, Rb is almost exclusively hosted in white mica, whereas N is also present in other phases in variable amounts. Rb in white micas does not correlate with N (Fig. 2). Instead, N correlates with Cs in some samples, suggesting that NH_4^+ may behave more similarly to Cs.

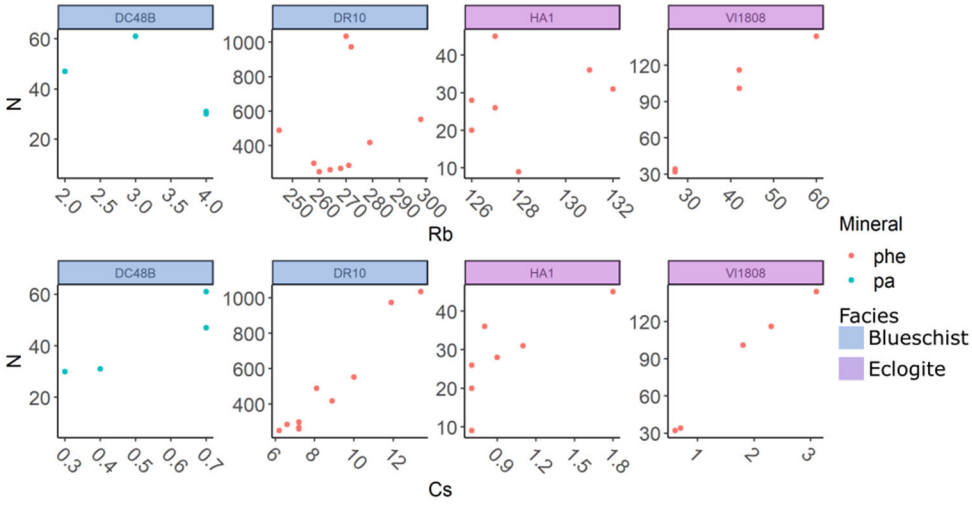

Fig. 2. Nitrogen versus Rb (top) and Cs (bottom) in white micas from selected samples. N correlates poorly with Rb but shows some correlations with Cs.

Bulk data shows that significant N is still present in K-poor samples, and the SIMS data shows that the N may be hosted in other phases (e.g amphibole, chlorite). There is also the possibility that some N is hosted in sealed voids and cracks since some high N analyses of these phases correspond with cracks in the grains. Work is ongoing to combine the SIMS data with bulk element concentrations and mineral modes to better understand the distribution of N between different phases.

References

[1] Bebout et al. (2013) Elements 9, 333-338
[2] Halama et al. (2017) Int Geol Rev 59, 702-720
[3] Harris et al. (2022) Geochim Cosmochim Acta 321, 16-34
[4] Mallik et al. (2018) Earth and Plan Sci Lett 482, 556-566

Making 4 billion year old glass

A. Hastie

School of GeoSciences, University of Edinburgh, Edinburgh EH9 3JW, UK

Rationale

The Eoarchaean and early Paleoarchaean Eras, 4.0-3.5 Ga, represent the period in Earth history when the Earth's oldest preserved continental crust was generated. The birth of the first continents modified the planet's interior and crustal surface. Volcanism, linked to initial continental growth, also compositionally affected the early atmosphere-hydrosphere exogenic reservoir and may have provided prebiotic molecules needed for the origin and evolution of life. Consequently, the initial formation of the continental crust is one of the most fundamental steps in the physical, chemical and biological evolution of the Earth and, yet, we still do not know how the first continental material was derived.

Geological Background and Strategy

5-10 million years after planetary accretion and the moon forming impact the Earth had magma ocean(s) that solidified and differentiated into a ~25-45 km thick basaltic crustal lid. After ~4.0 Ga, poorly understood geological processes began forming the earliest *preserved* continental crust. Eoarchaean to early Paleoarchaean Tonalite and Trondjhemite (EPTT) rock suites (plagioclase-rich "granites") represent the bulk of the earliest continental crust. Thus, to determine which rock-type partially melted to generate the first continental crust, we have to investigate the formation of the EPTT. Here we investigate if oceanic plateau material akin to the crustal lid can undergo partial melting at low pressures (≤1.4 GPa: ≤45 km) to form EPTT. High pressure-temperature experiments were undertaken on oceanic plateau starting compositions from 1.2-1.4 GPa and the melt pools were analysed on the Cameca 7f-Geo.

Results

Analyses show that partial melts at low pressures do not have compositions that match EPTT (Fig. 1). As such, shallow tectonic environments such as crustal resurfacing or asteroid impacts cannot be responsible for the oldest continents. Only deeper subduction environments are viable.

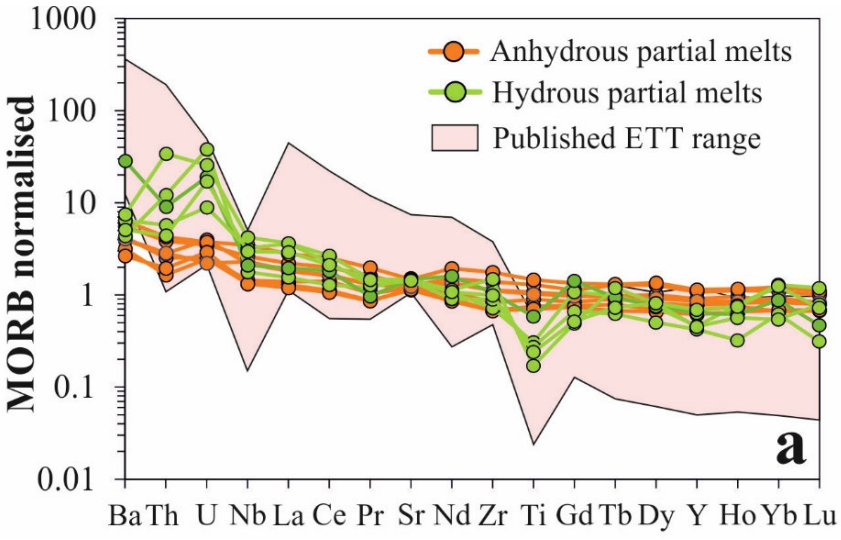

Fig. 1. Trace element spider diagram showing composition of experimental glasses compared to published ETT.

Chalcophile metal outgassing from Vanuatu volcanoes

O.R. Hogg[1], M. Edmonds[1], J. Blundy[2], F. Jenner[3] & B. Kunz[3]

[1] Department of Earth Sciences, University of Cambridge, UK
[2] Department of Earth Sciences, University of Oxford, UK
[3]School of Environment, Earth and Ecosystem Sciences, The Open University, MK7 6AA, UK

Background

Magmatic-hydrothermal fluids exsolved from magmas generated at convergent margins are enriched in a suite of metals, that can be largely attributed to their hydrous and chlorine-rich nature compared to other tectonic settings [1,2]. The more oxidised nature of arc magmas results in low sulfide proportions and promotes sulfide-undersaturated conditions throughout fractional crystallisation, which ultimately inhibits the extraction chalcophiles from the melt into the sulfide phase. The relationship between magmatic chlorine, water and sulfur contents and the metal contents of magmatic fluids and the conditions required to maximise them are contentious. How are maximum metal concentrations and fluxes of magmatic fluids generated? To investigate this we chose to model a series of hypothetical arc systems with varying magmatic water and chlorine contents including natural analogues of a water-rich basaltic arc (Mount Etna) and water-poor basaltic arc (Mount Yasur) with comparable Cl contents. We couple this with a detailed study of volcanoes along the Vanuatu arc. Mount Yasur is moderately enriched in Cl (~500 ppm) [3] whereas Ambae volcano records the highest dissolved Cl content in olivine-hosted melt inclusions (~7000 ppm) [4]. Can differences in magmatic Cl and H2O along the arc account for the variation in volcanic metal outgassing signatures? To answer these questions requires insight to the volatile and trace element systematics through a study of Yasur and Ambae whole rock and melt inclusions (MI's). Raman Spectroscopy was performed on bubble-bearing MI's hosted within olivine, clinopyroxene and plagioclase phenocryst from Yasur and Ambae.

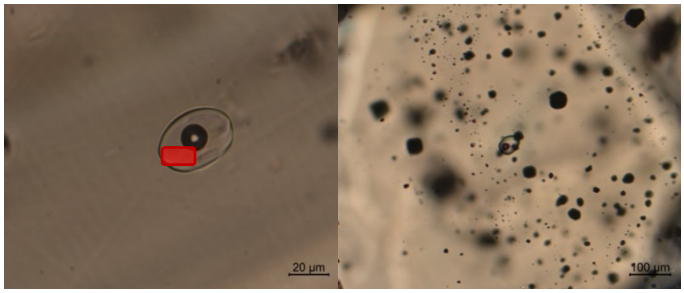

Fig. 1. Typical texture of olivine phenocrysts from Ambae. Dense populations of micro melt inclusions (<10 um) plus bubble-bearing MIs that ranged from 15-35 um. Red square outlines the SIMS pit area. Due to position of the bubbles, analyses would either intersect bubble and/or host crystal.

Melt inclusions from Yasur ranged from 40-150 um whereas those from Ambae were typically 15-40 um and a significant proportion of the bubble-bearing Ambae MI's were <30 um. Raman densities acquired from vapour bubble analysis were low and suggested low CO_2 concentrations that were indicative of extensive volatile degassing.

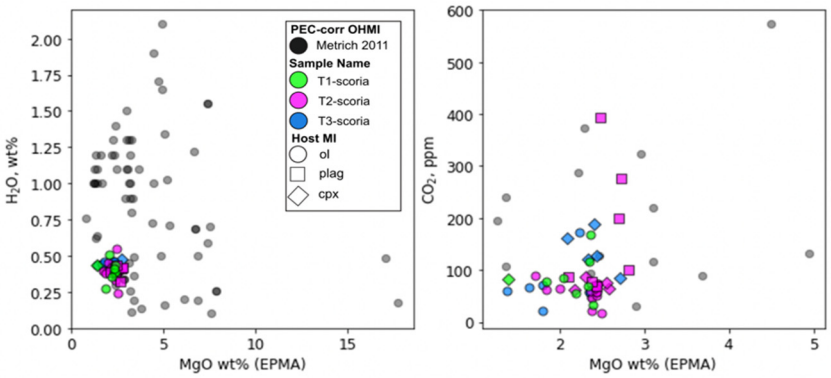

Fig. 2 Volatile concentrations in Yasur melt inclusions. Data from this study are coloured by sample name and symbols refer to phenocryst host. Compared to our data, published OHMI data [3] shown in grey have higher H_2O and similar CO_2 concentrations, at a given MgO contents.

Preliminary Results and Interpretations

Following Raman Spectroscopy, 220 MI's were prepared for SIMS analysis. Due to the smaller size of the Ambae MI's and the volume of the bubble they accommodated (Fig. 1), SIMS measurements were unsuccessful and this set of samples were discarded from the study. The remaining Yasur MI's (n=100) were analysed for H2O, CO2 and Ba, La and Ce, which after filtering and comparison with EPMA data, left 68 MI. H_2O concentrations range from 0.25 to 0.55 wt%, which for a given MgO content, are lower than published datasets (Fig. 2). CO_2 concentrations range from 40 and 400 ppm - similar to published OHMI data [3]. Following SIMS, EPMA data were collected, and PEC corrections calculated using the model of [5] which returned up to 6.5% PEC (Fig. 3). Isobars were plotted to give an indication of the storage/equilibration pressures recorded by our samples and degassing paths were estimated using solubility model MagmaSat [6] through VESIcal [7] (Fig. 4). Converting the maximum H_2O-CO_2 concentration MI pair to pressure, gives 300 bar which is significantly shallower than estimated depth of Yasur magma chamber [3] and further suggests that our samples have experienced extensive degassing.

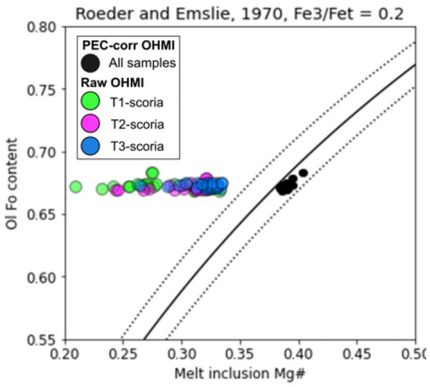

Fig. 3. OHMI PEC corrections and assessment of host-melt inclusion equilibrium. Raw OHMI data show a broad Mg# range for a relatively uniform olivine host Fo#. Post-PEC corrections shift OHMI's towards higher Mg#. Using the Roeder and Emslie (1970) model, OHMI's sit within the equilibrium field.

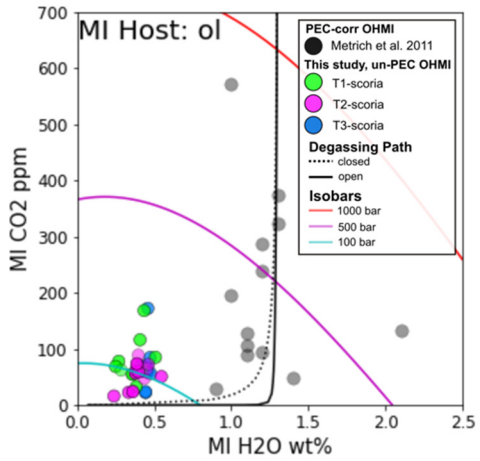

Fig. 4. Isobars and magma degassing pathways. OHMI data from this study are colored according to sample name and published data are shown in grey. Open system where all fluid is fractionate (solid), closed system where no fluid is lost (dotted) and closed system where magmas begin with 1.2 wt% H_2O [3].

References

[1] M. Edmonds, T.A. Mather and E.J. Liu (2018) Nature Geoscience **11** (10), 790-794
[2] O.R. Hogg, M.Edmonds, J. Blundy (2023) Earth and Planetary Science Letters (in press)
[3] N. Métrich et al. (2011) Journal of Petrology **52** (6), 1077-1105
[4] Y. Moussallam et al. (2019) Contributions to Mineralogy and Petrology **174,** 1-24
[5] L.V. Danyushevsky et al. (2000) Contributions to Mineralogy and Petrology **138**, 68-83
[6] M.S. Ghiorso and G.A.R. Gualda (2015) Contributions to Mineralogy and Petrology **169**, 53
[7] K. Iacovino et al. (2021) Earth and Space Science **8**, e2020EA001584

Exploring the volatile content of magmas driving eruptions at Rabaul caldera, Papua New Guinea

M. Höhn, B. McCormick Kilbride & M. Hartley

Department of Earth and Environmental Science, University of Manchester, Manchester, M13 9PL, UK

Background and Objectives

The Rabaul Caldera Complex (RCC) has historically been the most active volcano in Papua New Guinea. Rabaul is capable of large volume, high intensity caldera-forming eruptions as well as low intensity but more frequent intra-caldera eruptions. Any eruption at Rabaul poses a serious risk to local communities [1].

Previous studies at the RCC have revealed persistent and prodigious gas emissions, even between eruptions [2,3]. It is unknown why Rabaul is such a strong emitter of volcanic gases. Nevertheless, limited satellite-based observations of SO_2 emission [2,3] and studies of melt inclusions in the 1994 and 2006 eruptions products indicate that magmatic volatiles play a key control on the dynamics and strength of volcanic eruptions as well as the eruption style at the RCC [4,5].

Our objective was to quantify the pre-eruptive volatile content of magmas involved in the 2014 eruption of Tavurvur, the most recent eruption at the RCC. By comparing our new data with previous analyses of the 1994 and 2006 eruption products, we aim to build a time series describing the composition and evolution of Rabaul magmas, focusing on changes in volatile content.

Results

We used the 7f instrument to measure H_2O, CO_2, SO_2 and selected trace elements in 94 naturally quenched, glassy plagioclase-, clinopyroxene-, and olivine-hosted melt inclusions (MIs) and matrix glasses. Major elements, Cl and F were measured afterwards by electron microprobe at the University of Muenster in Germany. Post-entrapment crystallisation (PEC) corrections were carried out for all melt inclusions by adding the host mineral composition incrementally back into the melt inclusion until the equilibrium K_D value between melt and mineral was reached.

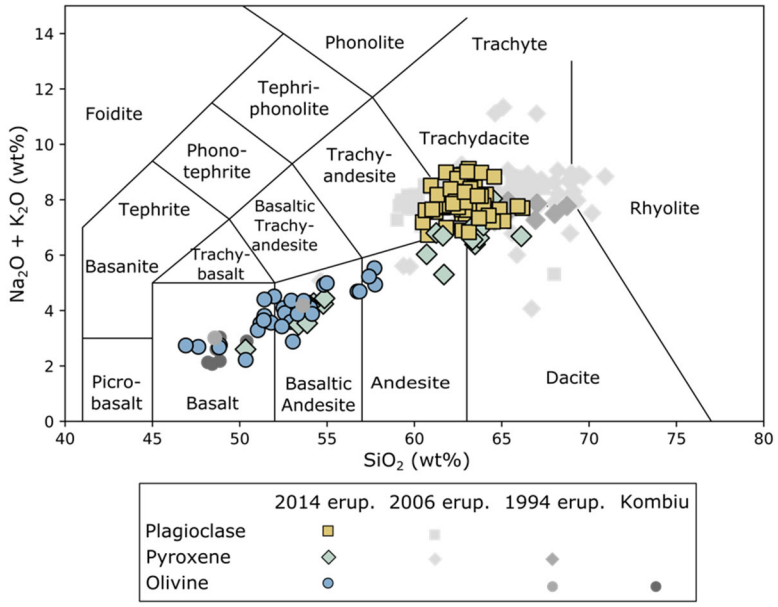

Fig. 5. TAS diagram comparing melt inclusions in the 2014 eruption products with those of previous eruptions and the nearby mafic volcano Kombiu [4, 5]. Shown here is PEC corrected data.

Melt inclusions in olivine have basaltic to basaltic andesite compositions (46.9–57.6 wt% SiO_2) whereas melt inclusions in plagioclase show more evolved compositions (62.7–66.2 wt% SiO_2). Overall, melt inclusions in the 2014 volcanic bombs follow the same geochemical trend as MIs in previous eruption products (Fig. 1). It has been previously proposed that this trend is the result of both fractional crystallisation as well as mixing of a resident dacitic magma body with basaltic recharge magma [1,5].

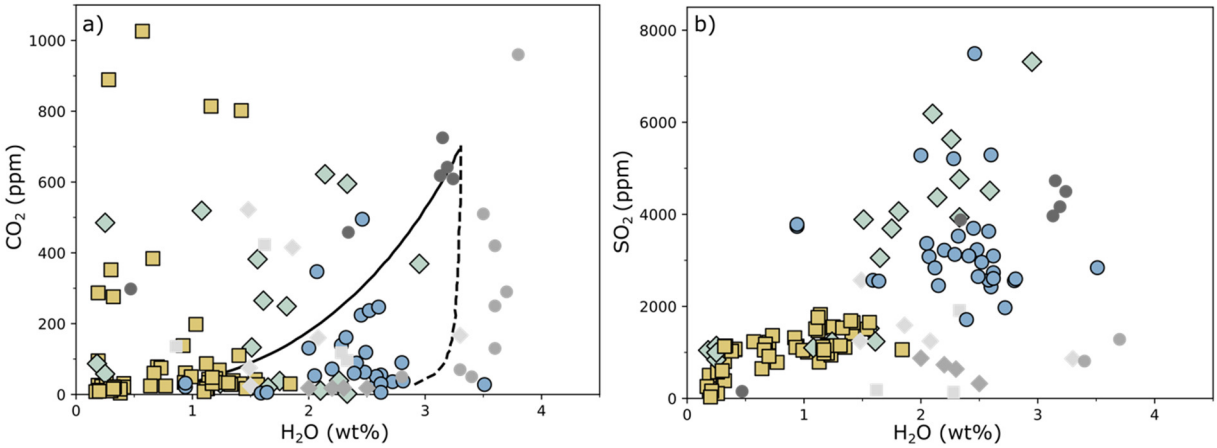

Fig. 6. Comparison of a) H_2O and CO_2 and b) H_2O and SO_2 contents between 2014 eruption products (coloured symbols) and samples of previous eruptions (grey symbols) [4,5]. Closed- and open-system degassing paths are shown with bold and dashed lines [5]. Symbols and colours as in Fig. 1. Shown here is PEC corrected data.

H_2O and SO_2 concentrations in olivine-hosted melt inclusions are higher (1.59–3.51 wt% H_2O, 1713–7493 ppm SO_2) than in melt inclusions in plagioclase hosts (0.17–1.84 wt% H_2O, 32–1832 ppm SO_2) (Fig. 2). Clinopyroxene (cpx)-hosted MIs display a wide range in both species from 0.18 to 2.95 wt% H_2O and 842 to 7315 ppm SO_2. Overall, the SO_2 content in all melt inclusions decreases with increasing SiO_2 concentration which was previously interpreted as reflecting crystallisation under volatile-saturated conditions [5].

While most plagioclase-hosted melt inclusions have CO_2 contents below 400 ppm, a group of four MIs in plagioclase show the highest CO_2 concentrations of all measured melt inclusions (802–1386 ppm CO_2). Olivine- and cpx-hosted MIs display CO_2 from 4 to 495 ppm and 2 to 622 ppm, respectively. However, caution must be exercised by interpreting the CO_2 contents of the analysed melt inclusions as additional CO_2 in fluid bubbles has not yet been accounted for.

In comparison, melt inclusions from the 1994 and 2006 eruptions have higher H_2O concentrations, whereas melt inclusions from the 2014 eruption extend towards higher CO_2 concentrations (at low H_2O content) and especially higher SO_2 values.

Future Work

Microscopy of the 2014 melt inclusions revealed frequent fluid bubbles, which form when post-entrapment crystallisation within an inclusion causes CO_2 to be released from the melt. We will determine the CO_2 content of fluid bubbles in the melt inclusions by Raman spectroscopy and then add the CO_2 contained in the fluid bubble to the CO_2 contained in the glass, to obtain the total CO_2 concentration for each melt inclusion.

References

[1] Fabbro G et al. (2020) J Volcanol Geotherm Res 393:106810
[2] McCormick B et al. (2012) Geochem Geophys Geosys 13:Q3008
[3] Carn S et al. (2017) Sci Rep 7:44095
[4] Roggensack K et al. (1996) Science 273:490-493
[5] Bouvet de Maisonneuve C et al. (2015) Geol Soc London Spec Publ 442:17-39

Magmatic volatile systematics in the 2020-21 St Vincent eruption and controls on hazardous effusive-explosive transitions at arc volcanoes

T. Howe[1], H. Tuffen[1], T. Christopher[2,3] & S. Moune[4,5]

[1]Lancaster Environment Centre, Lancaster University, Lancaster, LA1 4YQ
[2]Montserrat Volcano Observatory, Montserrat, West Indies
[3]Seismic Research Centre, UWI, West Indies
[4]Laboratoire Magmas et Volcans, Clermont-Ferrand, France
[5]Institut de Physique du Globe de Paris, France

Summary

H_2O and CO_2 were measured in 14 melt inclusions from La Soufriere & Soufriere Hills volcanoes in the Lesser Antilles, to characterise eruption-controlling volatile systematics and magma storage depths.

Systems studied

La Soufriere Volcano, St Vincent (SStV) There are 8 recorded eruptions between 1700s and 2021. Repose intervals of the previous 6 recorded explosive eruptions shorten from 140 to 42 years[1], indicating magmatic plumbing system changes.

H_2O and CO_2 contents in melt inclusion (MI) glasses of the products of the 2021 explosive eruption were collected via SIMS, together with MI bubble CO_2 (Raman), and sulphur, halogen and major element compositions (EPMA). This provides the first MI volatile dataset for the 2021 explosive eruption and first insights into SStV magma storage depths based on H_2O-CO_2 systematics. Earlier studies relied on H_2O only, compositional trends, or experimentally defined phase relations.

Soufriere Hills Volcano, Montserrat (SHV) SHV has undergone 5 phases of eruption from 1995-present. Published MI CO_2 concentrations are <60 ppm for phase 1 quartz and plagioclase[2] and ≤1032 ppm for phase 5 plagioclase and opx[3], yielding equilibrium pressures of 100-300 MPa. Our pilot data on phase 5 (2010) MI glass (Fig. 1) yields MI glass CO_2 and H_2O concentrations that closely match the range of previous studies (CO_2 ≤1032 ppm; H_2O ≤ 6.4 wt %). However, we have found that the majority (80-90 %) of the MI CO_2 resides in vapour bubbles, as proposed by other studies[4-5], and addition of this bubble-hosted CO_2 provides total MI CO_2 of ≤3500 ppm, >3x higher than any previous SHV analysis (Fig. 3). Our pilot data demonstrate the importance of including bubble-hosted CO_2 and have set the scene for a funded full proposal (Oct 2022 round).

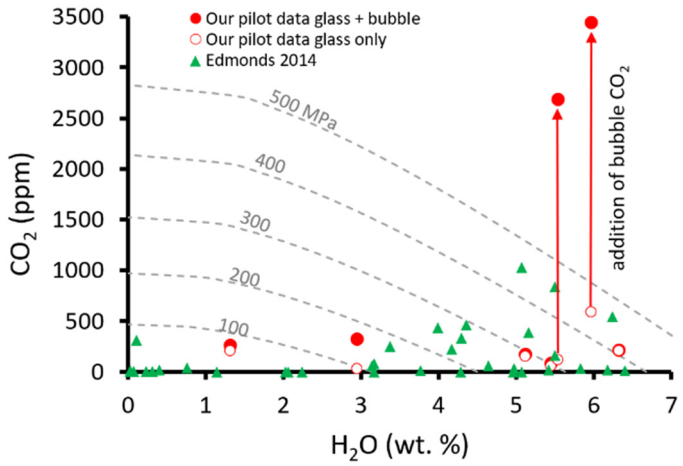

Fig. 1. Published SHV MI H_2O and CO_2[3] and our pilot data. While the range of H_2O and glass CO_2 contents are similar, addition of bubble-hosted CO_2 indicates significantly higher total CO_2 in two plag-hosted MIs (arrows). The solubility pressures are approximated using VolatileCalc.

References

[1] P. Cole et al. (2019) Journal of Volcanology and Geothermal Research **371**, 86-100
[2] Barclay et al. (1998) Geophysical Research Letters **25-18**, 3387-3541
[3] Edmonds et al. (2014) Geological Society, London, Memoirs, **39**, 291–315
[4] Wieser et al. (2020) Geochemistry, Geophysics, Geosystems, **22-2**
[5] Moore et al. (2015) American Mineralogist, **100-4**

Carbonate-bearing apatite in carbonatites and associated melts

M.C.S. Humphreys[1], M. Anenburg[2] & J.C.M. de Hoog[3]

[1]Department of Earth Sciences, Durham University, Science Labs, Stockton Road, Durham, DH1 3LE, UK
[2]Research School of Earth Sciences, Australian National University, 142 Mills Road, Acton, ACT 2601 Australia
[2]School of Geosciences, University of Edinburgh, Grant Institute, James Hutton Road, Kings Buildings, EH21 9FE

Scientific Report

Apatite crystals were analysed for ^{1}H, ^{12}C, $^{16}O^{1}H$, ^{19}F, ^{25}Mg, ^{30}Si, ^{31}P, ^{35}Cl and ^{44}Ca using the Cameca IMS-7f-Geo at IMF. Analyses were performed in low mass resolution mode using a 5 nA, 5 kV $^{16}O^{-}$ beam with a -75V offset applied. A 120 second pre-sputter with a 10 um raster area was used to clean the sample surface prior to each spot analysis. Analyte abundances were normalised to ^{44}Ca. Absolute volatile concentrations were retrieved by linear calibration of $X/^{44}Ca*CaO$ against a suite of seven previously characterised apatite standards [1,2], except for ^{1}H which showed a non-linear calibration (Fig. 1). The calibration apatites have water contents ranging from 0 to 1.40 wt% H_2O and carbon contents up to 0.81 wt% CO_2.

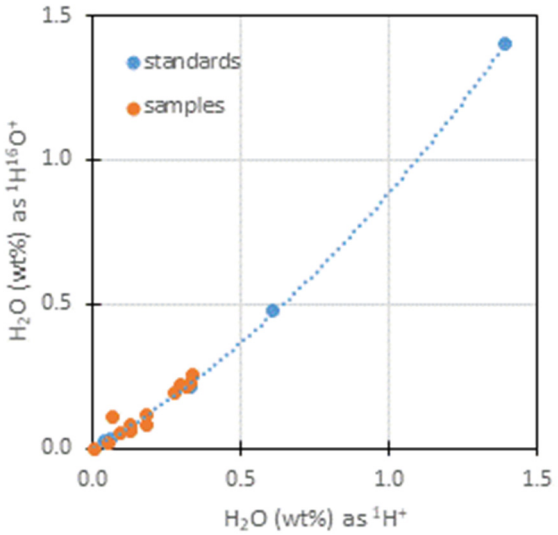

Fig. 1. Comparison of H_2O measured as ^{1}H and $^{16}O^{1}H$ using linear calibrations, showing non-linear response of ^{1}H.

An experimental carbonatite sample, synthesised at high P,T from carbonate, oxide and chloride powders, contains 2.60 ± 0.08 wt% CO_2, 0.21 ± 0.02 wt% H_2O, 0.57 ± 0.01 wt% F and 2.35 ± 0.07 wt% Cl. Combined with EPMA analysis for major and minor elements, this composition indicates a purely Type-B carbonate apatite (i.e. CO_3^{2-} accommodated on the phosphate site) with significant vacancies on the channel volatile site. CO_3^{2-} is mostly accommodated by a coupled substitution for PO_4^{3-} involving SiO_4^{4-}, but with a significant fraction (7-18%) of the carbonate coupled by F^{-}:

e.g., $Ca^{2+} + F^{-} = REE^{3+} + CO_3^{2-}$ [Eq. 1]

Carbonate concentrations were also analysed in apatites from two previously published studies reporting anomalously high-F compositions by EPMA. Electron microprobe analysis is susceptible to analytical artefacts that affect fluorine counts, whereas SIMS is not [3]. One of the apatites (VHDL) is objectively enriched in fluorine (4.3-4.9 wt% F) and also contains up to 0.6-0.9 wt% CO_3^{2-}. This indicates Type-B carbonate apatite (i.e., accommodated on the P-site) in a substitution such as [Eq. 1]. Stoichiometric calculations indicate that there is no CO_3^{2-} on the channel volatile site. The other (PAN) has normal F contents that are consistent with end-member fluorapatite (3.7-3.9 wt% F) and negligible dissolved CO_3^{2-}. These contrasting results emphasise the importance of accurate (SIMS, or time-corrected EPMA) analysis of halogens in apatite.

Both VHDL and carbonatite apatite appear to show pure Type-B substitutions, which means that further work may be needed to allow experimentally defined K_Ds for mixed Type-A/B carbonate apatite [2] to be applied to natural apatite crystals grown from carbonatite magmas. Finally, the carbonatite apatite bears some significant similarities to mantle apatites in lherzolite samples, which are interpreted to form through fluid metasomatism [4]. This reinforces that apatite shows promise to help define the carbonate compositions of magmatic and metasomatising fluids.

References

[1] Stock et al. (2018) Journal of Petrology **59**, 2463-2492
[2] Riker et al. (2018) American Mineralogist **103**, 260-270
[3] Stock et al. (2015) American Mineralogist **100**, 281-293
[4] O'Reilly & Griffin (2000) Lithos **53**, 217-232

Compositional profiles in plagioclase macrocrysts from the Fagradalsjall CE2021 eruption, Iceland

J. Maclennan

Dept. of Earth Sciences, University of Cambridge, Cambridge CB2 3EQ, UK

Background

The 2021 eruption at Fagradalsfjall in SW Iceland has been the focus of intense geological, geophysical, petrological and geochemical study. This ion-probe project was linked to a NERC Urgency grant which aimed to use microanalytical study of the crystal cargo of this eruption to inform the geophysical monitoring strategy in the region during the event. Petrological results show that the magma supply was from a storage reservoir close to the base of the crust, at about 14 km depth [1]. Shallow geophysical signals associated with the magmatic unrest were first recorded in early 2020, about 14 months prior to the eruption onset in late March 2021. Olivine and plagioclase macrocrysts from tephra samples were characterised by BSE and EDS mapping prior to acquisition of electron probe data from 51 profiles across plagioclase. An initial paper has already been published based on combining our electron probe profiles of plagioclase crystals with olivine data from a collaborating group in Heidelberg [2]. This work demonstrated that diffusion chronometry fits to Mg-Fe in olivine and Mg-in-plagioclase recovered timescales dominantly coincident with shallow geophysical unrest. This match indicates a connection between reconfiguration of the deep magmatic system with shallow earthquakes. It is important to note, however, that about 15% of the timescales in olivines extended to times prior to monitored geophysical unrest.

Ion Probe Targets

The initial plan was to use the ion probe data in conjunction with the electron probe work. The opportunity to publish rapidly in collaboration with the Heidelberg group and the unavoidable delays and logistical challenges associated with COVID restrictions meant that the ion probe data has not yet been published. It will form part of an ongoing study to better understand longer-term evolution in storage conditions in the Fagradalsfjall system. A subset of the 51 plagioclase profiles were chosen for ion-probe analyses, with a particular focus on the acquisition of diffusion profiles from elements that diffuse at different rates in plagioclase (e.g. Li, Mg, Sr). The analyst was John Craven for these sessions due to COVID restrictions preventing access to the lab for external PIs. Careful documentation of the samples and visual guides to the preferred profile locations allowed us to obtain good data.

Step Scan Profiles

Step scans with 2-4 micron spacing were acquired for 18 profiles. Ion yields relative to Si were calibrated each day. Counts on Ca and constraints from plagioclase stoichiometry were used to estimate true Si concentrations and thus to convert counts into concentrations for a suite of trace elements. The high spatial resolution of the step scans does come at some cost in terms of accuracy and long-term precision, but individual profiles show that short-term precision is sufficiently good to clearly identify spatial patterns in trace element contents (Fig 1). The shapes of the Mg profiles are in good agreement with available EPMA data. Shorter profiles in Sr, extending 20-30 microns into the cores of the crystals are consistent with diffusion times of a year or less between exposure of that boundary to new conditions and eruption. Fast-diffusing lithium appears to exhibit diffusion lengths greater than that of the scanned profiles. These data will be fit with a combined diffusion model (DFENS) and the inclusion of multiple elements will reduce the uncertainty in the fit below that derived from Mg alone.

Point Analyses

In order to convert the step scan profile shapes into better constrained absolute profiles, a number of point analyses were placed adjacent to the profiles with longer counting times and larger spot sizes. Typically 3 points were added per profile. These absolute concentrations are useful when establishing the initial conditions, and changes in boundary conditions, and likely temperatures for the diffusion modelling. Furthermore, when partition coefficients are available, comparison of core and rim concentrations indicates that the trace element contents of the liquid from which the rim grew was different to that in equilibrium with the cores. For example, the rims for profile G20210321_PL3A have a Sr concentration of about 140 ppm, while the core is closer to 90 ppm. This information will allow us to associate the diffusion timescales with the supply of deep-sourced enriched mantle melt to a near-Moho magma body, as described by Halldórsson [1].

Next Steps

The step scans will be calibrated with the point data and then used as an input for diffusion chronometry models. This work will provide tighter constraints on the timescales of unrest in the deep magmatic system and, combined with the trace element record of changes in host melt composition, will illuminate the causes of overturn of magmatic mushes in the build-up to the eruption.

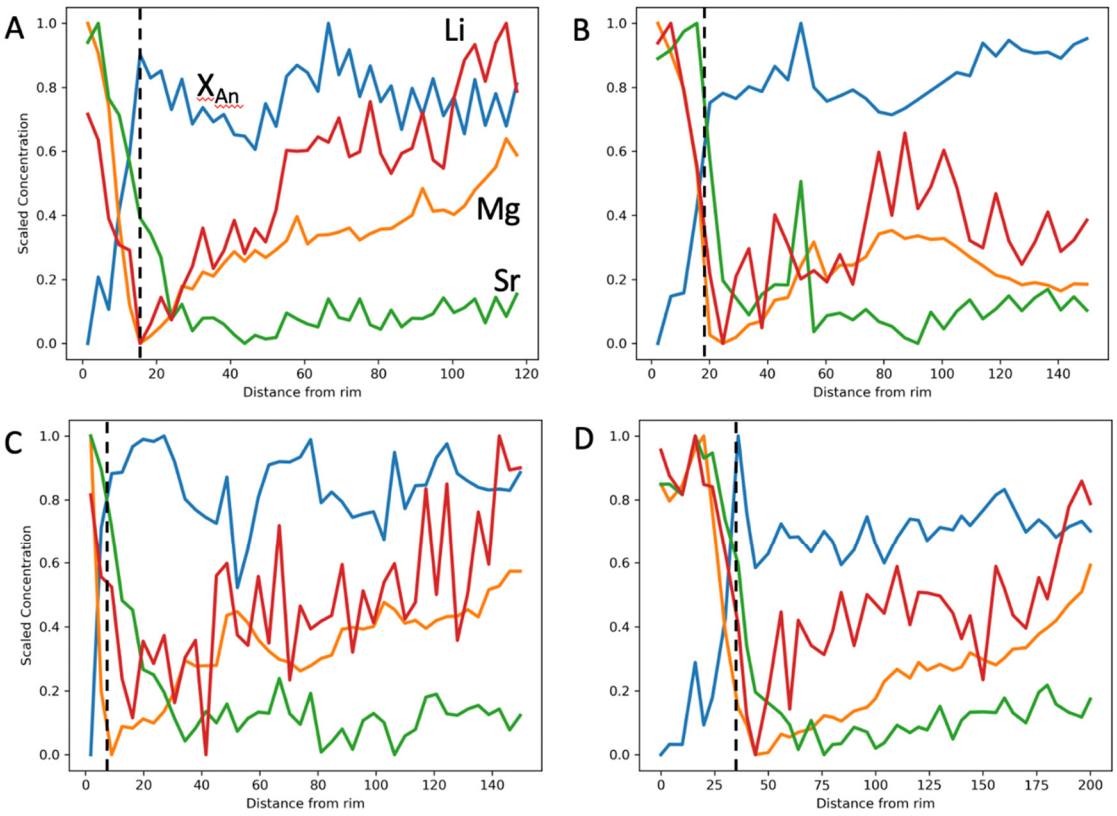

Fig. 1. Examples of step-scan data, scaled to [0,1] with anorthite content in blue, Mg in orange, Sr in green and Li in red. The distances are shown as a function of microns from the rim. The vertical dashed line shows estimated position of boundary between rim zone and higher anorthite core zone. Mg and Li show evidence for diffusional profiles that extend from 60 to >100 microns in from the rim/core boundary. Sr diffusion profiles into the core are also observed on a lengthscale of 10-30 microns. A) Mount3_PL17 B) G20210321_PL9 C) G20210321_PL11 _scale D) G20210321_PL3A

References

[1] S.A. Halldórsson et al. (2022) Nature **609**, 529-534
[2] M. Kahl et al. (2023) Geology **51**, 184-188

Life in deep fractures: evidence from Scandinavian boreholes

S. McMahon[1], H. Drake[2], J. Parnell[3], C. Heim[4], A. Boyce[5]

[1]School of GeoSciences, University of Edinburgh
[2]Department of Biology and Environmental Science, Linnæus University
[3]School of Geosciences, University of Aberdeen
[4]Institute of Geology and Mineralogy, University of Cologne
[5]SUERC

Background

Microbes in rocks and sediments underground and beneath the seafloor (the "deep biosphere") dominated the planet's biomass prior to the rise of land plants [1], and still contain more carbon than any other biome except forests. However, geological records of ancient subsurface microbial life are sparsely sampled and poorly understood, which hampers efforts to reconstruct long-term geosphere-biosphere interactions. Sulphate-rich fractures and veins may be favoured sites for microbial activity in the subsurface because sulphate is a widely used electron acceptor for anaerobic bacterial metabolism. This metabolism has the potential to produce several biosignatures, including sulphide minerals preserving a biogenic sulphur isotope composition. In a previous pilot study with the NERC IMF, SM found sulphur isotope evidence that microcrystalline pyrite in Mars-analogue gypsum veins hosted by Permian sedimentary rock has a subsurface bacterial origin [2]. This additional (8 hour) pilot IMF examined pyrite grains extracted from older gypsum veins through bedrock in the Fennoscandian Shield. Sample material consists of hand-picked pyrite grains from three sites (Laxemar boreholes, 822 m and 971 m deep; Garpenberg Mine, 300 m+; Falu Mine, 300 m+) in Sweden.

Work done

We used the IMF to assess the sulphur isotope composition ($\delta^{34}S$) of the pyrite. Host gypsum $\delta^{34}S$ has previously been measured for the Laxemar localities; for the other localities it was obtained at SUERC by collaborator Adrian Boyce as part of this project. The small scale SIMS spots enabled high spatial control of the d34S variability within the pyrite grains, which turned out to be minimal. Nevertheless, larger-scale laser analysis would have been too crude for analysing these small grains.

Results and further work

We observed that the sulphur isotope composition of the pyrite ($\delta^{34}S$) was lighter (up to tens per mil) than that of the gypsum occurring in the same veins. This result constitutes promising evidence in favour of the hypothesis that the pyrite sulphide was produced by bacterial sulphate reduction. This research project is ongoing. Independent insights into biological activity in these ancient veins will be provided by lipid biomarker analyses of the host gypsum by collaborator Christine Heim, still to be completed.

References

[1] McMahon, S., & Parnell, J. (2018) Journal of the Geological Society **175 (5)**, 716-720.
[2] McMahon, S., Parnell, J., & Reekie, P. B. R. (2020) Astrobiology **20 (10)**, 1212-1223.

Basaltic andesite derived by mantle melting beneath Kluchevskoy volcano, Kamchatka

E. Melekhova & J. Blundy

Dept. of Earth Sciences, University of Oxford, Oxford OX1 3AN, UK

Introduction

It is commonly accepted that starting point for subduction zone magmatism is partial melting of mantle wedge peridotite fluxed by fluids derived from the subducted slab. Although Mg-rich basalt is one of the most common products of this type of mantle melting, a variety of other mantle-derived primitive arc magmas, ranging in composition from high-Mg andesite to picrite, has been recognised based on geochemistry and experimental petrology[1]. This variety reflects changes in the thermal state of the underlying mantle wedge and the supply of water from the slab. Understanding source depth of primitive magmas has implications for thermal modelling of subduction zones and interpretation of geophysical data.

Constraining the depth from which a given magma was sourced is a challenge in igneous petrology. Several strategies can be utilized to constrain the depth from which a given magma originated. Here we use experiments to determine the point of multiple saturation on the liquidus of an erupted magma. The starting point of multiple saturation concept is an assumption that at its source a melt was in equilibrium with a polymineralic rock. Ideally, the number of co-saturating minerals is such that the thermodynamic variance of the system is very low. Experimentally constrained multiple saturation point defines the pressure and temperature at which the erupted melt could be extracted from a polymineralic source rock. However, for the experiments being meaningful the petrological and geochemical constrains of mantle xenoliths and erupted magmas, estimate of fO_2 and volatile budget are required.

Kluchevskoy is one of the most active volcanos on Earth, yielding roughly biannual eruptions of predominantly basaltic andesite magmas. This compositional consistency of erupted magmas suggests buffering of the magma composition either by mantle or crustal lithology. To explore the conditions of magma generation beneath Kluchevskoy we used inverse experimental approach to constrain multiple saturation point on the liquidus surface of high-MgO basaltic andesite (KLU-96-03[2]).

We have performed 32 near liquidous, equilibrium piston-cylinder experiments between 0.5 and 1.0 GPa under hydrous (3 and 6 wt% H_2O) conditions at ΔNNO+1. All experiments were fluid undersaturated. The major element compositions of experimental phases were analysed by electron microprobe analyses on Cameca SX-5 FE at University of Oxford using standard calibration techniques with oxides and silicates. Volatile contents of experimental glasses were analysed by secondary ion mass spectrometry (SIMS) at the NERC ion microprobe facility, University of Edinburgh, using a Cameca IMS 7f-Geo instrument with a nominal 10 kV primary beam of $^{16}O^-$ ions and 5nA beam current. H_2O and CO_2 were calibrated against synthetic basaltic glass standards[3].

Results

The experimental results are presented on Figure 1. Our data was supplemented by experimental data on very similar high-MgO basalt starting composition from Volcan Jorullo, Mexico[4]. Weaver et al. carried out near liquidous experiments between 1.0 and 2.0 GPa with initial H_2O content 3, 5 and 7 wt%.

We show that high-MgO basaltic andesite with 3.5 ±0.5 wt% of H_2O is multiply saturated with lherzolite assemblage (ol (Fo_{90}) + cpx + opx + Cr-spinel) close to its liquidous (melt fraction ≥ 90) at 0.60±0.05 GPa (23±2 km depth) and 1220-1240ºC (Fig. 1). Thus, experimental results indicate that high-MgO basaltic andesite was produced by partial melting of peridotite source and a primary, undifferentiated magma. These results are in a good agreement with geophysical studies of Kluchevskoy that show magmas are

supplied directly from a reservoir at a depth of 25-30 km through a nearly vertical pipe-like conduit[5]. These results provide a tight constraint on the thermal structure of the mantle wedge beneath Kluchevskoy. The mantle wedge temperature obtained in these experiments are higher than typical temperatures used for thermal models[6] suggesting that upwelling asthenosphere might directly impinge the Moho in a similar fashion to mid-ocean ridges.

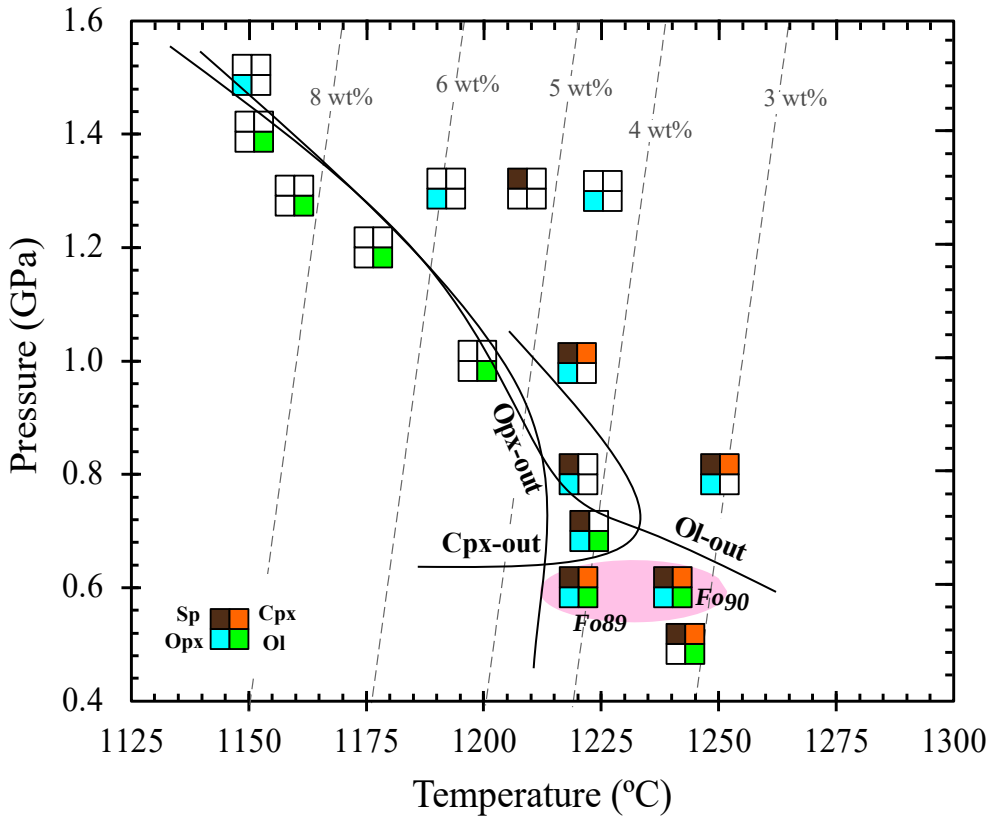

Fig. 1. Liquidus surface diagram for high-MgO basaltic andesite (KLU-96-03) used to define the liquidus multiple saturation point. Only experiments with ≥90% glass are plotted. The olivine composition (mole% Fo) marked next to experiment. Liquidus contours (dashed grey lines) are labelled with the corresponding H_2O content of the melt. The pink shaded area defines high-MgO basaltic andesite liquidus multiple saturated with lherzolite composition.

References

[1] Schmidt & Jagoutz (2017). Geochemistry, Geophysics, Geosystems 18/8, 2817-2854
[2] Churikova et al. (2001). Journal of Petrology 42(8), 1567-1593
[3] Shishkina et al. (2010). Chemical Geology 277:115–125
[4] Weaver et al. (2011). Earth and Planetary Science Letters 308, 97–106
[5] Kulakov et al. (2017). Journal of Geophysical Research Solid Earth, 122, 3852-3874
[6] Syracuse et al. (2010). Physics of the Earth and Planetary Interiors 183 (2010) 73–90

Apatite inclusions in zircon reveal water-saturated, crystal-rich magma reservoirs beneath porphyry copper deposits

Chetan Nathwani[1,2], Simon Large[1], Emily Brugge[1,2], Jamie Wilkinson[1,2] & Yannick Buret[1]

[1]Department of Earth Sciences, Natural History Museum, London, SW7 5BD, UK
[2]Department of Earth Science and Engineering, Imperial College London, London, SW7 2AZ, UK

Introduction

Large volume, intermediate-felsic magma reservoirs are the source of melt and mineralising fluids which generate porphyry copper deposits - the source of most of society's copper. Cooling and crystallisation of such magmas are thought to play a key role in driving the exsolution and expulsion of a magmatic volatile phase. During fluid saturation, certain metals (e.g. Cu, Au and Mo) are preferentially partitioned into the fluid phase relative to the melt and the metalliferous fluids are released into surrounding rock to form a porphyry Cu deposit. The timing of fluid saturation in a magma are expected to play an important role in controlling the location, size and grade of porphyry deposits.

Constraining the behaviour of volatiles during the evolution of magmatic systems is challenging, because volatiles will saturate and escape the petrological record. In addition, many studies rely on the study of melt inclusions, which may experience post-entrapment modification, or be rarely preserved, as is the case for the strongly hydrothermally altered igneous rocks. One increasingly popular method to constrain magma volatile evolution is using the composition of igneous apatite which is unique in that it incorporates three of the important ore-forming components: water, chlorine and sulphur. However, studies have shown that halogens in apatite are highly susceptible to re-equilibration with hydrothermal fluids [1]. Therefore, in this study we analysed apatite inclusions in zircon, which are shielded from hydrothermal re-equilbration. We analysed apatite inclusions in zircon from rocks with pre- (the Yarabamba Batholith - 67-59 Ma) and syn-date porphyry Cu mineralisation (the Quellaveco porphyry – 58-55 Ma). We aimed to track changes in fluid saturation and volatile behaviour in the Myr prior to and during porphyry Cu mineralisation to constrain processes which may be conducive to porphyry Cu mineralisation.

Methods and Results

Representative samples of Yarabamba and Quellaveco intrusive rocks were selected for apatite compositional analysis. Apatite inclusions in zircon were analysed from zircon grains from 12 different samples which were mounted in epoxy.

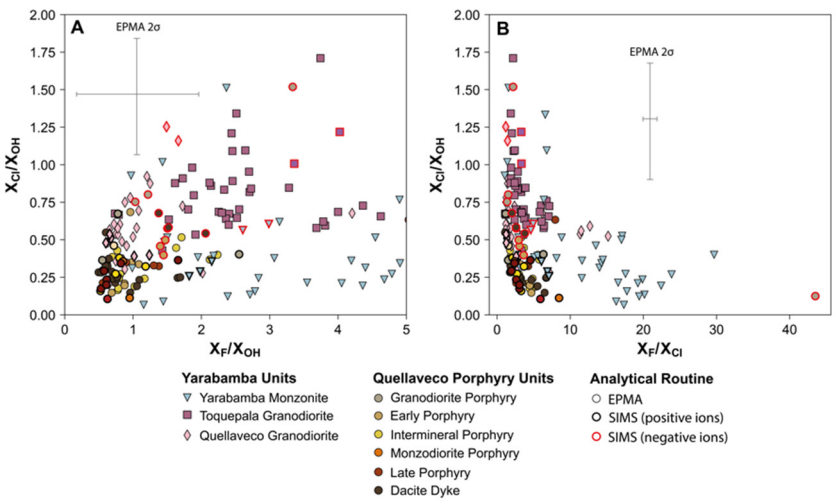

Fig. 1. Overview of apatite inclusion in zircon compositions for all Quellaveco and Yarabamba rocks measured by EPMA and SIMS.

Major element electron probe microanalyses (EPMA) of inclusion apatites were conducted at the Natural History Museum, London. Secondary ion mass spectrometry (SIMS) was performed at the NERC EIMF to measure Cl, F, OH and CO_2. The rationale behind using SIMS was to 1) quantify OH which otherwise can only be estimated from EPMA data (stoichiometrically) and thus reduce uncertainty and 2) provide the first (to our knowledge) measurements of carbon in apatite from a porphyry copper deposit since

the role of CO_2 in ore-forming events is unknown [2]. Two analytical approaches were used: the first was conducted using a Cameca IMS 7f ion microprobe using an approximate spot size of 10 µm, low $^{16}O^-$ primary beam current. Because this approach yielded a small number of successful analyses due to large spot size and high detection limits, a second approach was used. This involved use of the Cameca IMS 1270 at using a Cs^+ beam. The main challenges of this project were the small size of apatite inclusions relative to the beam size (yielding fewer successful analyses than expected) and the high background concentrations likely caused by degassing of epoxy (which led to high detection limits for OH).

Discussion

In general, we found a good agreement between EPMA and SIMS data for apatite inclusions in zircon (for Cl and F) and reasonable agreement between OH measured directly by SIMS and OH estimated by difference using EPMA data. Only six out of seventeen analyses (Cs^+ method) gave CO_2 concentrations above detection limit, however some of these extended up to 5 wt.% CO_2 which is impossible within apatite. Higher concentrations occurred close to cracks suggesting contamination. Thus, in general the CO_2 of these apatites was found to be low <0.04 wt.% in line with shallow apatite crystallization from intermediate-felsic melts (with no evidence for CO_2 fluxing).

Apatite inclusions from the Quellaveco porphyries show homogeneous compositions, characterised by both lower F and Cl than those from the Yarabamba Batholith. In general, overall differences between samples are present in data obtained by both EPMA and SIMS. Estimated OH values from EPMA are consistent with those measured directly by SIMS. The characteristically low Cl/OH and low F/OH ratios of apatite inclusions in the Quellaveco porphyries, relative to the Yarabamba Batholith, may indicate crystallisation from a magma that was low in Cl and F and/or high in OH (Fig. 1). This could be caused by the magmatic system being fluid saturated at the time of apatite and zircon crystallisation which would result in preferential removal of Cl over F and OH from the melt.

We designed a numerical model to explain our data, where we first invert apatite halogen ratios to melt halogen ratios using thermodynamic calibrations [3]. We then model water-saturated versus water-undersaturated melt evolution. Our model suggests that the Quellaveco porphyry apatites crystallised under water-saturated melt evolution (Fig. 2), whereas the precursor batholith is potentially water-undersaturated. Using Monte Carlo modelling the Quellaveco apatites record significant loss of fluid from the system, corresponding to a crystal-rich magma reservoir.

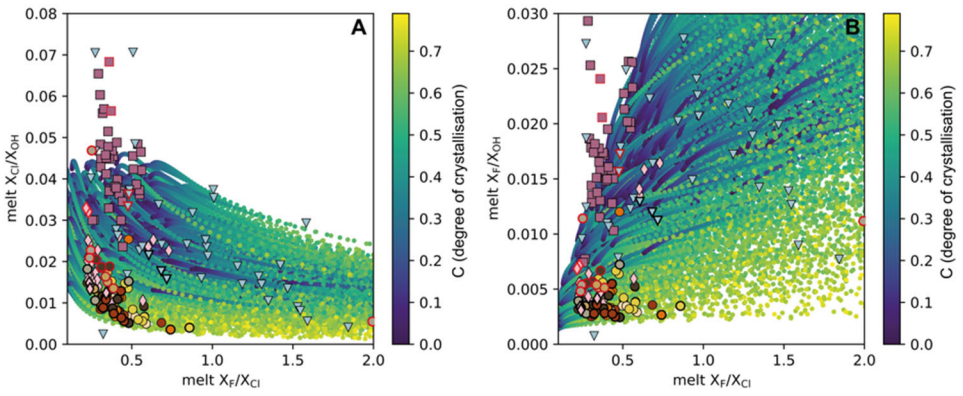

Fig. 2. Melt halogen ratios calculated from apatite (symbols) and Monte Carlo modelling of fluid-saturated melt evolution

In summary, we find evidence of a temporal transition towards fluid-saturated magma evolution coincident with porphyry Cu mineralisation, and evidence for a crystal-rich system. Such fluid-saturated crystal-rich magma reservoirs may play a key role in forming giant porphyry Cu deposits.

References

[1] F. Bouzari et al. (2016) Economic Geology **111**, 1397-1410
[2] J. Lowenstern (2001) Min. Dep., 36, 490-502
[3] W. Li & F. Costa, (2020) Geochimica et Cosmochimica Acta **269**, 203-222

Oxygen isotopes of laminated microspheres from the South Falkland Sediment Drift

V.L. Peck

British Antarctic Survey, High Cross, Madingley Road, Cambridge CB3 0ET

Rationale

Siliceous microspherules ranging in diameter from 100-300 mm are found in marine sediments collected from the South Falkland Sediment Drift, U1534, on IODP Expedition 3821. The microspheres were initially thought to be microtecktites, but upon embedding them in resin and polishing them it was found that the spherules were concentrically laminated. EDX further determined that they were almost pure silica and therefore inconsistent with then being microtektites.

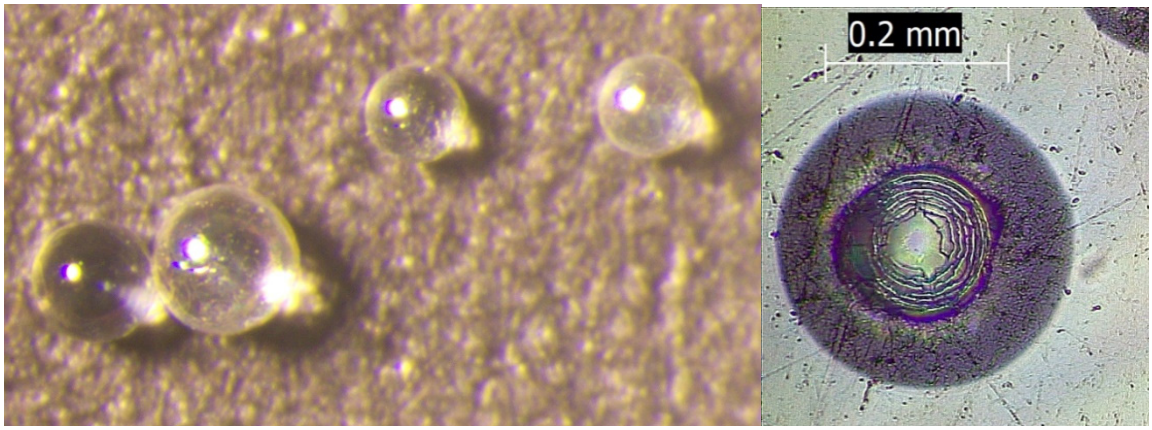

Fig. 1. Photograph of microspherules before (left) and after (right) mounting and polishing.

Results

To understand the origin of these spheres I proposed a pilot oxygen isotope study with the NERC IMF. The $\delta^{18}O$ of the silica was found to be 45.2+/-0.4 per mil (7 spot measurement on 2 spheres). These $\delta^{18}O$ values are consistent with the spheres being in equilibrium with ambient seawater/porewater at the core site.

An extensive review of literature on siliceous laminations eventually turned up one citation reporting morphometrically similar microspheres from surface sediments from the Ross Sea shelf [1]. We have since determined that the sediments from which the microspheres were found south of the Falklands were likely ~1 Ma. These microspheres are therefore contemporary with the Great Patagonian Glaciation when the Patagonian Ice Sheet reached its maximum extent. At this time glacial discharge entered the Atlantic Ocean. The common feature therefore between the microspheres deposited south of the Falklands at ~1 Ma and those found on the seafloor off the Ross Sea coast is their proximity to glacial, or subglacial, discharge. We are currently pursuing the hypothesis that these microspheres are formed within a subglacial setting. A tidally influenced setting, where silica-laden fresh waters cyclically exchange with sea water, may provide a mechanism to account for the accretion of multiple silica laminations. Further investigation into the chemistry and potential mode of formation of these microspheres is needed. However, should they be found to have formed in a subglacial environment these microspheres will confirm that marine-terminating glaciers on the Atlantic coast were a feature of the Great Patagonian Glaciation.

References

[1] IODP Publications • Volume 382 expedition reports • Site U1534

[2] Weiterman, S.D.; Russell, M.D.J. (1986) Antarctic Journal of the United States **21(5)**, 159-160

Generating economic rare earth element deposits through hydrothermal fluid-rock interactions

D. Price & I.B. Butler

School of GeoSciences, University of Edinburgh, Edinburgh EH9 3JW, UK

Scientific and Experimental Context

This report is for a pilot study to investigate whether ion microprobe methods can be applied to the analysis of complex, fine-grained mixtures of experimental products resulting from the reaction of rare earth element solutions with carbonate minerals at hydrothermal temperatures. The purpose of such experiments is to explore fluid-rock reactions and the impact of wall-rock composition on hydrothermal REE mineralisation. Some of the most economically significant REE deposits are associated with carbonatites of magmatic origin, or carbonate rocks of sedimentary origin where economic enrichment occurs predominantly through hydrothermal transport of REEs and deposition via the formation of REE fluorcarbonate ± REE phosphate minerals. Experiments replicating fluid-rock interactions leading to the formation of hydrothermal REE fluorcarbonates were conducted at up to 200°C for up to 20 days. Variations in both wall-rock and hydrothermal fluid compositions were considered to explore what parameters influence the distribution of LREE and HREE elements during the precipitation of REE fluorcarbonate minerals. XRD and SEM analyses of the products showed the formation of the mineral bastnäsite, which is the principal ore mineral for REEs in many carbonate systems. This pilot was targeted towards the determination of REE ratios in the synthetic products to compare with known REE ratios in the initial reactant solutions in order to establish the REE partitioning during hydrothermal fluid-rock mineralisation of REE bearing fluoro-carbonates.

For this pilot, we analysed a single sample synthesised at 200°C for 5 days with a 0.02 M REE solution. The REE ratio in the solution mirrored that of a natural hydrothermal fluid from the Okorusu carbonatites in Namibia [1]. The amounts used were as follows, in percentage of total REEs: (74% La, 25% Nd, 0.06% Dy, 0.26% Er, 0.17% Yb).

Analytical Methodology

Due to the semi-powdered nature of the sample, it was decided that the material to be analysed was to be pressed into indium and left under vacuum for 24 hours to stabilise. An initial attempt to analyse the crystals individually quickly proved unfruitful as the crystals were too small and too intimately mixed. Instead, the sample was analysed for seven 100 x 100 µm raster areas with a 13 kV beam. This proved adequate as the objective of the experiments was to obtain relative ratios of the REEs in the sample, to determine the LREE/HREE partitioning. The actual REE concentrations in the minerals were of secondary importance.

Attempts to make an internal standard by evaporating the REE starting solution onto silicon wafers proved untenable from a sample preparation perspective. As such, Durango apatite was used. After analysis, the isotopic counts were corrected for natural abundances and counts for elements not placed in the system were able to be attributed to REE oxide and REE fluoride interferences.

Results

The pilot study confirmed that the technique can be used to measure the relative ratios between the different REEs in the experimental product, although problems for the analysis of fine-grained mixed crystalline product remain. The SIMS data could not be used to directly attribute REE ratios to a specific mineral grain at this stage. Considerable interference correction was required, which could be remedied, in part by selection of REE elements at the experimental stage.

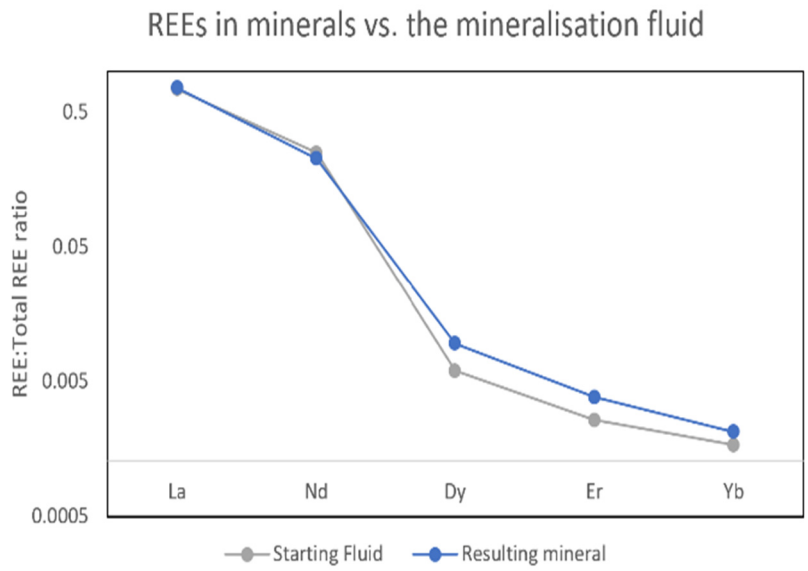

Fig. 7. The IMF pilot data in the context of the measured REE composition of the pre reaction fluids.

The results show that REE partitioning in the event of REE mineralisation via hydrothermal fluid interaction with a wall-rock is dependent on, but not wholly related to, the REE content of the mineralising fluid (Fig. 1). The results point to some fractionation of HREE between the precipitated minerals and the reaction solution. The solid phase incorporated more of the HREE compared to the starting solution and less La and Nd.

REE data are presented as the ratio of the measured REE counts to the total REE counts measured for the sample. This enables direct comparison of the SIMS data with similar REE ratios determined for the reactant solutions using ICP-OES (in that case the ratio of REE concentration in solution to the total REE concentration in solution).

References

[1] Bühn, B., Rankin, A.H., Schneider, J. and Dulski, P. (2002) Chemical geology, **186** (1-2), pp.75-98.

Generating economic rare earth element deposits through hydrothermal fluid-rock interactions

D. Price[1] & I.B. Butler[1]

[1]School of GeoSciences, University of Edinburgh, Edinburgh EH9 3JW, UK

Scientific and Experimental Context

Fluid-rock reactions and the impact of wall-rock composition on hydrothermal REE mineralisation were explored. Some of the most economically significant REE deposits are associated with carbonatites of magmatic origin, or carbonate rocks where economic enrichment occurs predominantly through hydrothermal reactions with carbonate-rich wall rocks (e.g. Bayan Obo [1], Mountain Pass [2]).

Experiments replicating fluid-rock interactions leading to the formation of hydrothermal REE fluoro-carbonates were conducted at up to 200°C for 20 days. Variations in both wall-rock and hydrothermal fluid compositions were considered to explore what parameters affected the precipitation of REE fluoro-carbonate minerals. The wall-rocks had varied dolomite, apatite and fluorite content (the fluorite was an experimentally convenient means of introducing fluoride to the system which is difficult in practice because of the low solubility of REE fluorides at ambient temperatures). La, Nd, Dy, Er and Yb were used as a representative suite of light to heavy REEs. REE mixtures ranged from binary combinations (eg. La-Nd, La-Er, Nd-Yb etc.) to full suites at equimolar ratios. REE concentrations in the starting solution also varied from 0.02 M to 0.2 M. XRD and SEM analyses of the products showed the formation of the economically important minerals bastnäsite, monazite and xenotime for certain wall-rock and fluid combinations. REE fluoride precipitates were also present.

Our aim was to measure the REE ratios of the synthesised products to determine the REE partitioning during hydrothermal fluid-rock mineralisation of REE bearing fluoro-carbonates and REE phosphates. Some questions were (1) How does the wall rock composition influence the partitioning of LREE and HREE into the minerals? (2) To what extent do the LREE and HREE partition within the resulting minerals?

Analytical Methodology

Following the protocol developed during a pilot study, the material was pressed into indium and five 100 x 100 µm raster areas were analysed with a 13 kV beam for each sample. The isotopes measured were 139La, 143Nd, 162Dy, 167Er and 171Yb as well as 19F, 24Mg, 31P, 35Cl and 40Ca. The REE isotopes were chosen specifically to not have any interferences with fluorides or oxides of other REEs.

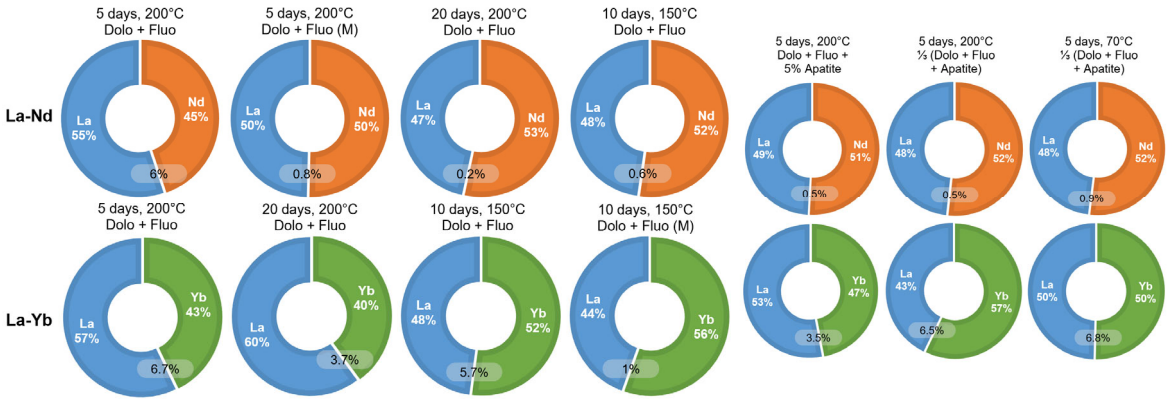

Fig. 8. *REE ratios in the solids for La-Nd and La-Yb experiments (% REE in final mixture). Standard errors of the mean of the repeat SIMS measurements on the same sample are shown on the charts. This value represents the uncertainty for each REE in the ratio. e.g. the top left La-Nd experiment with a 50:50 starting ratio resulted in a solid with a 55:45 ratio. Taking into account the 6% uncertainty, the ratio in the solid could possibly range between 49:51 and 61:39.*

Results

Reactions with hydrothermal fluids with most binary REE combinations resulted in a broad 50:50 REE distribution in the solids. This was regardless of wall-rock or REE composition, duration or temperature (Fig. 1). Subsequent ICP-MS analyses of all supernatant solutions revealed that they contained approximately 0.1% of the total REE from the starting solution. Thus REE utilisation (i.e. transfer from an initial aqueous condition to a precipitated mineral) over the experimental durations examined was near 100%. Consequently, the measured REE distribution variations in the experimental products are highly unlikely to result from solid-solution partitioning.

Figure 1 does indicate that some partitioning between REEs from binary mixtures was observed where the measured variation in REE distribution from the 50:50 reactant ratio exceeds the analytical error. X-ray powder diffraction data (not shown in this report) indicate the presence of REE fluoride precipitates as well as REE fluoro-carbonates and phosphates, and SEM observation of the reaction products indicates that the crystalline precipitates are intimately mixed and fine grained. We speculate that measured REE mixtures in the final product that deviate significantly from the 50:50 starting mixture may result from i) REE fractionation between fluoro-carbonate and fluoride or phosphate reaction products and ii) unequal sampling of mixed phases during analysis of 100 x 100 µm areas.

One experiment with equal concentrations of La, Nd, Dy, Er and Yb produced bastnäsite and REE fluorides. Analysis showed a similar REE distribution to that of the starting solution but with a slight LREE enrichment (Fig. 2). Again the reaction yield with respect to the starting REE concentration was close to 100%, and the observed REE fractionation may result from different REE distributions between fluoro-carbonates and fluorides and unequal sampling of those phases during raster analysis.

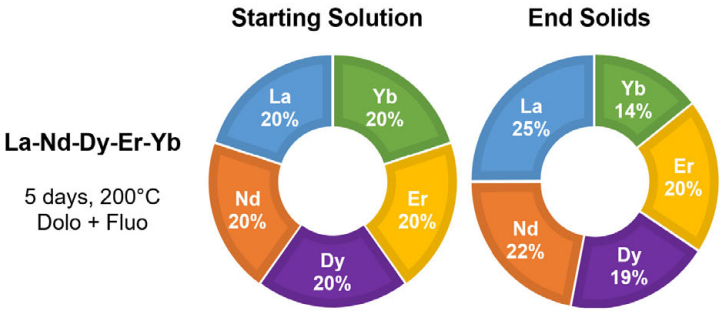

Fig. 9. *REE ratios in the starting fluid and post-experiment solids and liquids. Standard errors of the mean of the repeat SIMS measurements on the same sample are as follows: La 1.34%; Nd 0.53%; Dy 0.55%; Er 0.68%; Yb 0.66%*

The analytical methodology put in place by the IMF works, and is applicable to such experimental products which are troublesome or impossible to mount by conventional means. The results from analysis of the fine-grained, inter-grown and mixed composition precipitates that resulted from the synthetic experiments do appear to indicate variations of REE distribution between different precipitate phases. However the nature of the mixed component products means that the determination of how REEs partition between the experimental phases is qualitative at best.

References

[1] Ling, M.et al. (2013) Sci. Rep. **3**, 1776; DOI:10.1038/srep01776.
[2] Verplanck, P.L and van Gosen, B.S. (2011). USGS Open-File Report 2011–1256.

Insights into the volatile evolution of the Campanian Ignimbrite magmatic system using apatite compositions

V. Smith[1], M. Humphreys[2], R. Isaia[3] & J. De Hoog[4]

[1]Research Laboratory for Archaeology, University of Oxford, Oxford OX1 3TG, UK
[2]Department of Earth Sciences, Durham University, UK
[3]INGV, Osservatorio Vesuviano, Italy
[4]EIMF, School of Geosciences, University of Edinburgh, UK

Introduction

The Campanian Ignimbrite (CI) eruption from Campi Flegrei, Italy was the largest eruption in Europe in the last 200 ka. The Plinian phase and pyroclastic density currents (PDCs) erupted more than 155 km^3 of magma [1,2]. This research aims to gain new insight into this voluminous magmatic system by integrating new glass, clinopyroxene and apatite data with published petrological evidence. Our previous research on the smaller post-15 ka Campi Flegrei eruptions showed that apatite crystals are useful records of the evolution of the volatiles and indicated that melts remained volatile undersaturated until shortly before the eruption [3,4]. Here we use the volatile element compositions of apatite inclusions and microphenocrysts from the CI to establish the volatile history of the magmatic system that fed the enormous eruption.

In December 2019 we analysed major, trace and volatile elements in a representative suite of apatite inclusions within clinopyroxene phenocrysts and apatite microphenocrysts from samples taken through the CI eruption stratigraphy. Samples from the Plinian fallout and three different PDC units were analysed. These 2019 data showed that there were two compositionally distinct groups of apatite. In order to model these apatite data [cf. 4,5] we needed information on how the compositions changed over time. We supplemented our previous dataset with new analyses from apatite inclusions in biotite in early 2022. Biotite commences crystallisation after clinopyroxene [6], and thus provides information on how the volatile elements changed as the magmatic system evolved.

Analytical details

The CI apatite inclusions in biotite were analysed on the Cameca-7f with a 18 keV net impact energy (13 keV primary and 5 keV secondary) $^{16}O-$ primary ion beam. Most of the apatite crystals were analysed using 20 nA current that corresponded to a beam size of 10 microns. The current was reduced to 500 pA to provide a 2 micron beam and allow smaller apatite crystals to be analysed. ^{44}Ca was used as the internal standard for all analyses, and Ca contents were determined using a wavelength-dispersive electron microprobe at the University of Oxford. The apatite H_2O, CO_2, F and Cl concentrations were determined by generating calibration curves using the normalised (to ^{44}Ca) volatile counts collected on a range of natural and synthetic apatite standards.

Results

Matrix glass compositions of the deposits in and around the caldera and from distal sites indicate two largely homogenous melts were erupted [7]. The first Plinian phase erupted the most evolved melt (7.02–7.53 wt% K_2O; Magma 1) and another melt (9.45–10.26 wt% K_2O; Magma 2) was also tapped during the later PDC phases [4]. The evolved Magma 1 glasses are more abundant in both proximal and distal deposits implying that it was volumetrically larger than Magma 2. Published trace element and isotopic compositions indicate that these two melts are not linked by fractional crystallisation [8,9].

Crystals were extracted from the Plinian and PDC eruption deposits at various locations around the caldera. In addition to compositions of the apatite microphenocrysts, the major element composition of the melt inclusions (MI) and matrix glass around the biotite and clinopyroxene crystals were analysed. These melt compositions indicate that: (1) biotite only crystallised in the Magma 2; (2) a large proportion of clinopyroxenes started crystallising in the Magma 2 and then were transferred into the Magma 1, and some continued to crystallise while others, similar to the biotite crystals, did not; (3)

many clinopyroxene crystals crystallised entirely in Magma 1; and (4) some crystals crystallised in a more mafic melt that has not been detected in the deposits.

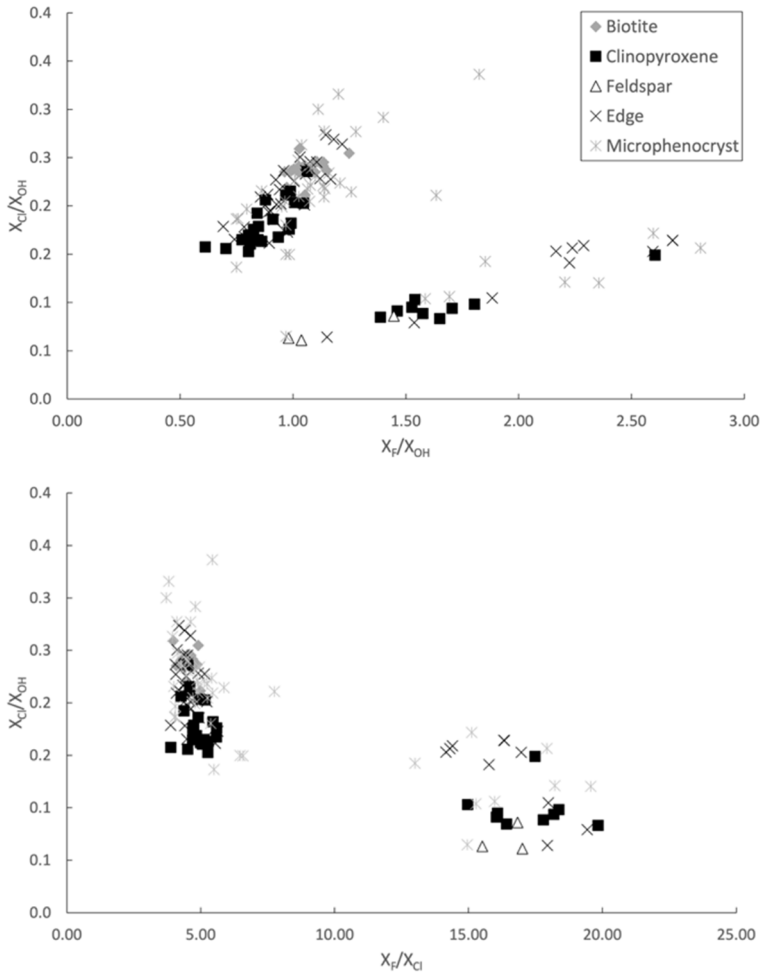

The volatile compositions of the apatite crystals within the CI deposits plot in two distinct groups (Fig. 1), and using MI hosted in the same crystals as the apatite inclusions we were able to relate the two apatite compositional groups to the two magmas. Apatite crystals in the Cl-rich group (Fig. 1) crystallised in Magma 2, and the F-rich apatites grew in Magma 1. The new biotite inclusion data provides the required temporal constraints and indicates that the volatile content of Magma 2 became enriched in both F and Cl over time.

Fig. 1. Volatile compositions of apatite inclusions in feldspar, clinopyroxene and biotite, as well as apatites partly included in crystals (labelled 'edge') and apatite microphenocrysts from the CI deposits. Data are plotted as mole fraction ratios. The Cl-rich (lower X_F/X_{Cl}) apatite group corresponds to the Magma 2 and vice versa.

Further work

Covid interrupted the labwork for this project and we were unable to obtain and prepare samples for analysis. We have recently completed more electron microprobe analysis on other inclusions to further constrain the temporal trends. Now that we have constrained the evolution of the volatile trends of the two magmas, we will use the numerical model of Humphreys et al. [5] to constrain the volatile evolution of the magmas. These apatite data will also be integrated other petrological datasets to constrain the amount of dissolved and exsolved gas in the magmatic system at the time of the caldera-forming eruption.

References

[1] A. Silleni et al. (2020) Frontiers in Earth Science **8**:543399.
[2] A. Costa et al. (2012) Geophysical Research Letters **39**, L10310.
[3] M.J. Stock et al. (2016) Nature Geoscience **9**, 249-255.
[4] M.J. Stock et al. (2018) Journal of Petrology **59,** 2463–2492.
[5] M.C.S. Humphreys et al. (2021) Earth and Planetary Science Letters **576**: 117198.
[6] G.A.R. Gualda et al. (2012) Journal of Petrology 53, 875–890.
[7] V.C. Smith et al. (2016) Bulletin of Volcanology **78**, 45.
[8] E. Tomlinson et al. (2012) Geochimica et Cosmochimica Acta **86**:318–337
[9] S. Di Salvo et al. (2020) *Lithos* **376–377**:105780

Sulfur cycling at subduction zones: sulfur isotopic composition of Aleutian Island melt inclusions

Z. Taracsák[1,2], T.A Mather[1], T. Plank[3], A. Auippa[4] & D.M. Pyle[1]

[1]Department of Earth Sciences, University of Oxford, Oxford OX1 3AN, UK
[2]Department of Earth Sciences, University of Cambridge, Cambridge CB2 3EQ, UK
[3]Lamont-Doherty Earth Observatory, Columbia University, Palisades NY 16094, New York, USA
[4]DiSTeM, University of Palermo, 90123 Palermo, Italy

Background and Motivation

The Aleutian Islands are located in the northern Pacific Ocean, where the Pacific plate currently subducts under the North American Plate. It is made up of numerous volcanic islands that form a chain more than 2000 km long between Alaska and Kamchatka Peninsulas (Fig. 1A).

Volcanoes located along the Aleutian arc erupt some of the most sulfur-rich magmas found on Earth today: melt inclusions (MIs) record sulfur contents up to 5000 ppm at a number of locations, including Augustine [1], Shishaldin and Makushin volcanoes (Fig. 2). Due to high sediment discharge from the rivers surrounding the Gulf of Alaska, the Aleutian Arc offers a unique location to explore how variations in sediment input to subduction zones may influence the sulfur cycling in volcanic arcs.

As part of project IMF714/0521, we analysed Li, B, volatile (H, C, S, F, Cl) contents and sulfur isotope ratios ($^{34}S/^{32}S$, expressed as $\delta^{34}S$ relative to V-CDT) using the IMS-1270 and 7f-geo instruments at Edinburgh. Analyses were carried out in glassy melt inclusions picked from four samples. These include scoria samples from Makushin volcano (Pakushin cone) known to contain up to 5000 ppm S [2], the 1977 eruption of Seguam [1], an older side cone (Virgin cone) and the 1999 eruption of Shishaldin [2]. These samples cover considerable variability in sediment flux along the arc (Fig. 1B), and also sample some of the most S-rich products on the Aleutian Arc, with MIs from the Shishaldin Virgin cone sample containing up to 5300 ppm S (Fig. 2).

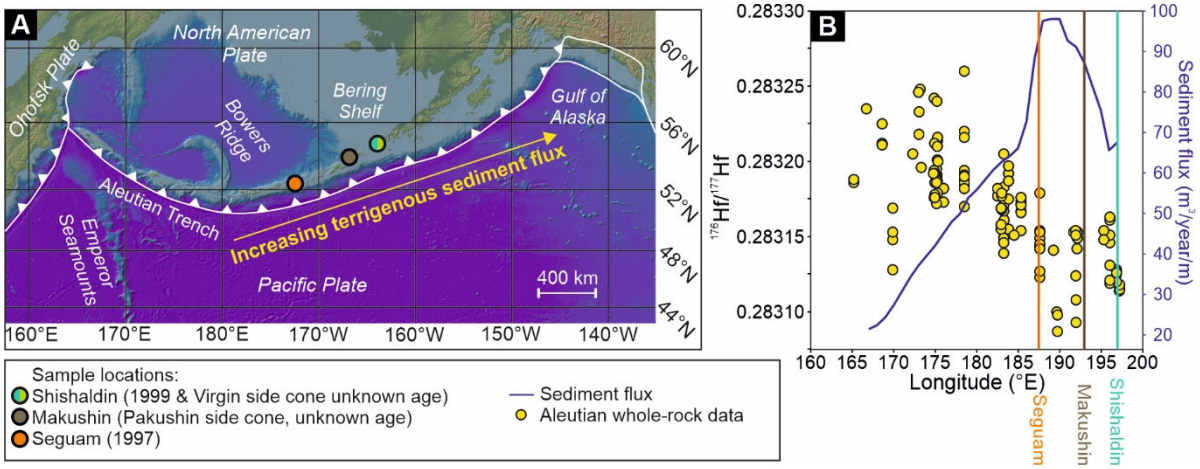

Fig. 1. (A) Map of the Aleutian Islands and surrounding areas. The location of the three volcanoes studied here are shown with filled circles. Note that from Shishaldin two locations were studied. The yellow arrow indicates the direction of increasing terrigenous sediment input to the present-day arc. (B) Hafnium isotope ratios measured from Aleutian volcanics plotted against the longitude of each sample [3]. Isotope data are taken from the GEOROC database (accessed on 15th March 2023). The blue line in (B) is the estimated sediment flux along the Aleutian arc, using values from [3] and reference therein. Enrichment in ^{177}Hf is thought to record increased addition of a sediment-derived component to the mantle wedge, which is in accordance with flux estimates.

Results and Discussion

So far, our work has been mainly focussed on the sulfur isotope composition of the Aleutian MIs. These data are shown in Fig 2., alongside calculated degassing models. Using the regression methodology of

[4], we find that gas-melt sulfur isotope fractionation factors ($\alpha_{g\text{-}m}$) at Aleutian volcanoes are between 0.997 and 1.000. Notably, this range is close to identical to that estimates for Central American volcanoes [4], indicating that progressive enrichment of volcanic gases in ^{34}S may be a widespread if not global feature. Furthermore, $\alpha_{g\text{-}m}$ shows a temperature dependence, as the lowest temperature sample studied here (Shishaldin 1999) shows the largest isotope fractionation.

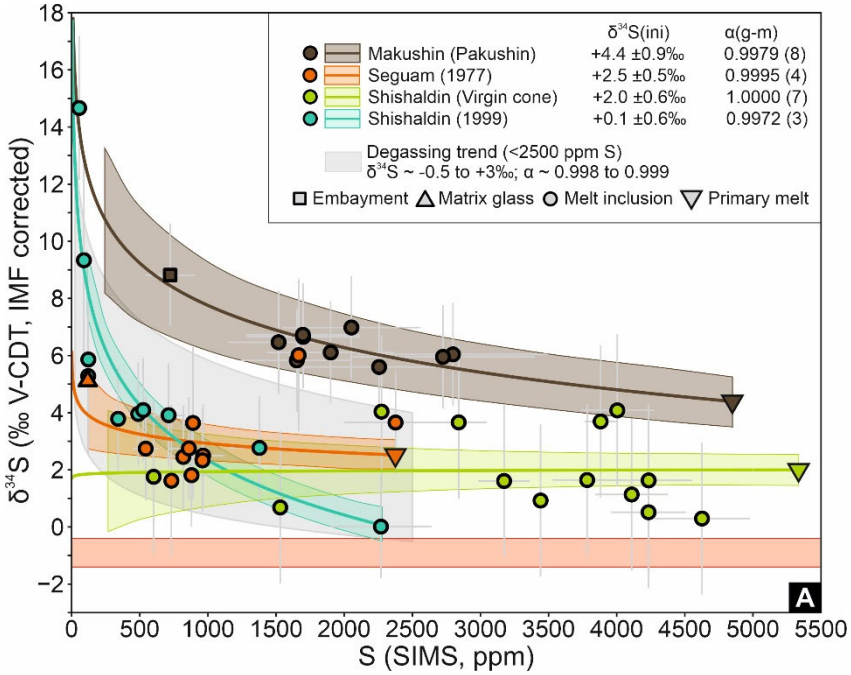

Fig. 2. Instrumental mass fractionation-corrected sulfur isotopic composition of Aleutian Islands melt inclusions and glasses vs. S content. Solid lines are modelled degassing pathways for each sample calculated using the regression methodology described in [4]. Using this method, and assuming that the most S-rich MIs measured from the samples represent the undegassed S content of the melt, a gas-melt S isotope fractionation factor ($\alpha_{g\text{-}m}$) and an undegassed melt $\delta^{34}S$ value (downward triangles) can be determined. The grey shaded area represents the evolution of melt with 2500 ppm S and assumes a fractionation factor between 0.998 and 0.999. All error bars are 2σ, while shaded areas are 1 standard error of the regression.

Undegassed melt $\delta^{34}S$ values are estimated to be between +0.1 and +4.4‰ (triangles in Fig. 2). These values are uniformly enriched in ^{34}S compared to the depleted mantle (red line in Fig. 2 [5]), and similar to those estimated at Central America (between +0.9 and +2.2‰ [4]). These data indicate that excess ^{34}S is added to the mantle wedge, potentially on a global scale. However, we find that melts with high undegassed S content may not necessarily be the most ^{34}S -enriched, as shown by the composition of melts from the Virgin side cone of Shishaldin. This sample has a lower undegassed $\delta^{34}S$ (2.0±0.6‰) compared to the similarly sulfur-rich Pakushin cone of Makushin volcano (+4.4±0.9‰). Mantle heterogeneity present prior to slab fluid addition may influence the S content and $\delta^{34}S$ of arc magmas, and it may be an important factor at Shishaldin, where F and Ti-rich melts are known to erupt, as recorded by MIs from the 1999 eruption. Our results also find that Makushin and Seguam have the heaviest undegassed melt $\delta^{34}S$ estimate out of seven samples (including three from Central America [4]) that have been investigated so far as part of this NSF-NERC project. These volcanoes are located near the maximum of observed sediment flux along the Aleutian arc (Fig. 1B), and may indicate that larger sediment input coincides with high $\delta^{34}S$ in arc magmas.

References

[1] M.M. Zimmer et al. (2010) Journal of Petrology **51:12**, 2411-2444
[2] D. J. Rasmussen (2019) PhD Thesis, Columbia University, p.200
[3] Yogodzinski G.M et al. (2010) Earth and Planetary Science Letters **300**, 226-238
[4] Taracsák et al. (2023) Earth and Planetary Science Letters **602**, 117948
[5] Labidi et al. (2013) Nature **501**, 208-211

H_2O solubility in trachydacite melt

A. Voigt[1] & M. Cassidy[1,2]

[1]Department of Earth Sciences, University of Oxford, South Parks Road, Oxford OX1 3AN, UK
[2]School of Geography, Earth and Environmental Sciences, University of Birmingham, Birmingham B15 2TT, UK

Introduction

Volatile solubilities in magmas can have a big impact on the explosivity of a volcanic eruption, as they control volatile nucleation and growth. During magma ascent towards the surface and therefore decompression of the magmatic system, volatiles expand and degas dependant on their solubilities, creating magmatic overpressures, and driving the magma ascent. Trachydacite magma systems, such as the 1257 eruption of Mt Samalas, Indonesia, have been responsible for some of the most explosive eruptions in recent Earth history. However, volatile solubilities in intermediate alkaline magmas are understudied despite the high eruptive potential of these systems. Here we analyse H_2O concentrations in experimental glasses under equilibrated and decompressed conditions using trachydacite pumice from the 1257 eruption of Mt Samalas as starting material. Experiments were performed under equilibrium conditions at 900°C, 25-200 MPa and at decompression rates between 0.1-15 MPa/s.

Objectives and hypotheses

H_2O solubilities in trachydacite (measured with SIMS) will be used to:

1) Investigate the exsolution path and transfer of dissolved H_2O into the gas phase;

2) Investigate whether H_2O is more likely to dissolve into trachydacite melt than into other magma compositions;

3) Test the accuracy of available solubility models for predicting H_2O solubility in trachydacite melts.

Results

Results show that H_2O concentrations in experiments decompressed from 150 to 50 MPa at 900°C and different decompression rates between 0.1 - 15.0 MPa/s show similar water contents (2.7 wt.% H_2O) than equilibrium H_2O solubilities at 50 MPa (2.3 wt.% H_2O) assuming early degassing at the investigated decompression (magma ascent) rates (Fig. 1a). In comparison to other magmatic compositions, water solubilities in trachydacite match the H_2O solubilities in other magmatic compositions (e.g. phonolite, latite) at pressures up to 100 MPa, but display overall low solubilities (about 4 wt.%) at higher pressures (Fig. 1b). H_2O solubility in trachydacite up to 100 MPa is described well by modern solubility models. At high pressures between 150 and 200 MPa, all solubility models overestimate H_2O solubility in trachydacite by 0.5 – 1.7 wt.% H_2O (Fig. 1c).

References

[1] M. Mangan & T. Sisson (2000) Earth and Planetary Science Letters, **183**(3-4), 441-455
[2] J. Berndt et al. (2002) American Mineralogist **87**,11-12
[3,4] V. Di Matteo et al. (2006) Chemical Geology **229.1-3**, 113-124
[5] G. Iacono-Marziano et al. (2007) Journal of Volcanology and Geothermal Research **161.3**, 151-164
[6] M. Ghiorso & G. Gualda (2015) Contributions to Mineralogy and Petrology, **169(6)**, 1–30
[7] G. Moore et al. (1998) American Mineralogist, **83(1)**, 36–42
[8] P. Papale et al. (2006) Chemical Geology, **229(1–3)**, 78–95
[9] S. Newman, S., & J. Lowenstern (2002) Computers & Geosciences, **28(5)**, 597–604
[10] Y. Liu et al. (2005) Journal of Volcanology and Geothermal Research, **143(1–3)**, 219–235
[11] T. Shishkina, etal. (2014) Chemical Geology, **388**, 112–129

Figure 1: see next page

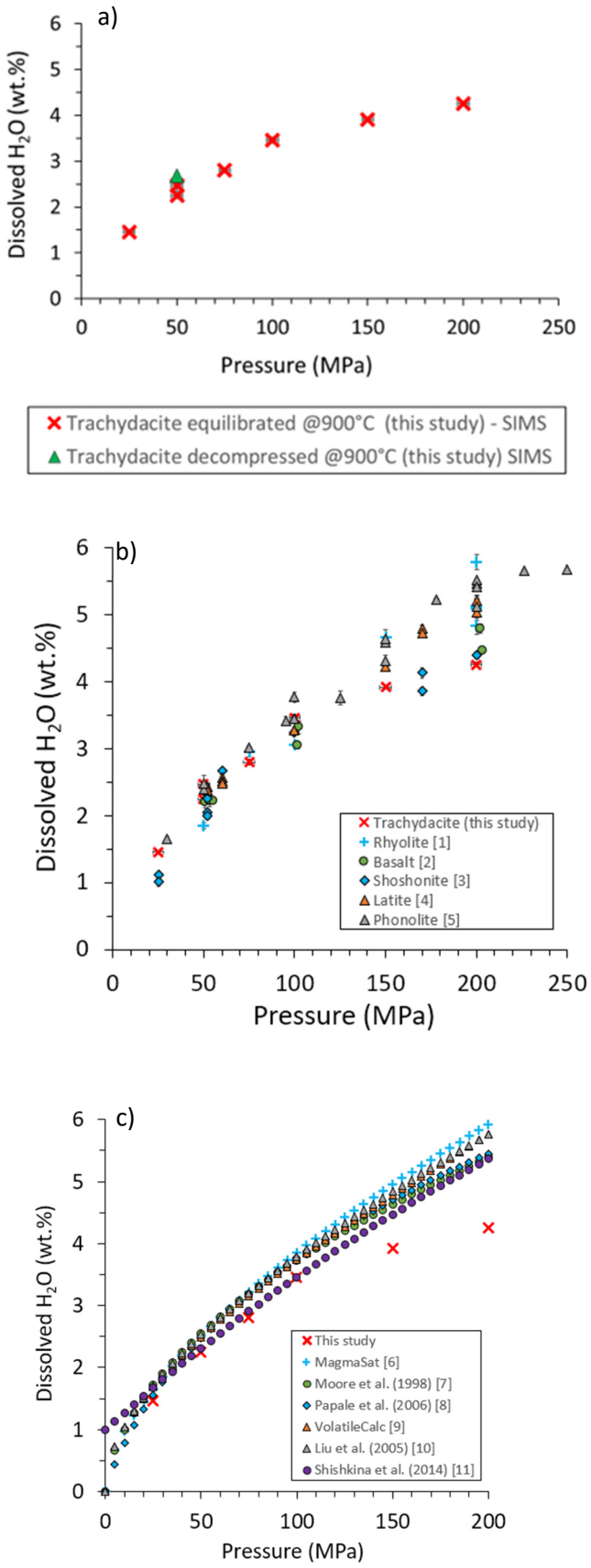

Fig. 1. H_2O concentrations in equilibrated trachydacite experiments, measured with SIMS, in comparison to a) amount of H_2O in decompressed trachydacite glasses b) H_2O in other magmatic compositions, c) solubility models.

Crustal intrusion of basaltic magmas in the Main Ethiopian Rift

K. Wong[1], D. Ferguson[1], P. Wieser[2], D. Morgan[1], M. Edmonds[3], A. Z. Tadesse[4], G. Yirgu[5], J. Harvey[1] & S. Hammond[6]

[1]School of Earth and Environment, University of Leeds, United Kingdom
[2]Earth and Planetary Science, University of California, Berkeley, United States of America
[3]Department of Earth Sciences, University of Cambridge, United Kingdom
[4]Department of Geosciences, Environment and Society, Université Libre de Bruxelles, Belgium
[5]School of Earth Sciences, Addis Ababa University, Ethiopia
[6]School of Environment, Earth and Ecosystems Sciences, The Open University, United Kingdom

Introduction

Continental rifting involves the rupture of strong continental lithosphere to form new ocean basins, and often involves intrusion of substantial volumes of magma into the rifting crust [1–3]. Magmas can accommodate extension via dyke intrusion and can alter the thermo-mechanical nature of the crust [4–6], facilitating continental breakup; however observational constraints on basaltic intrusion depths in active rifts are lacking.

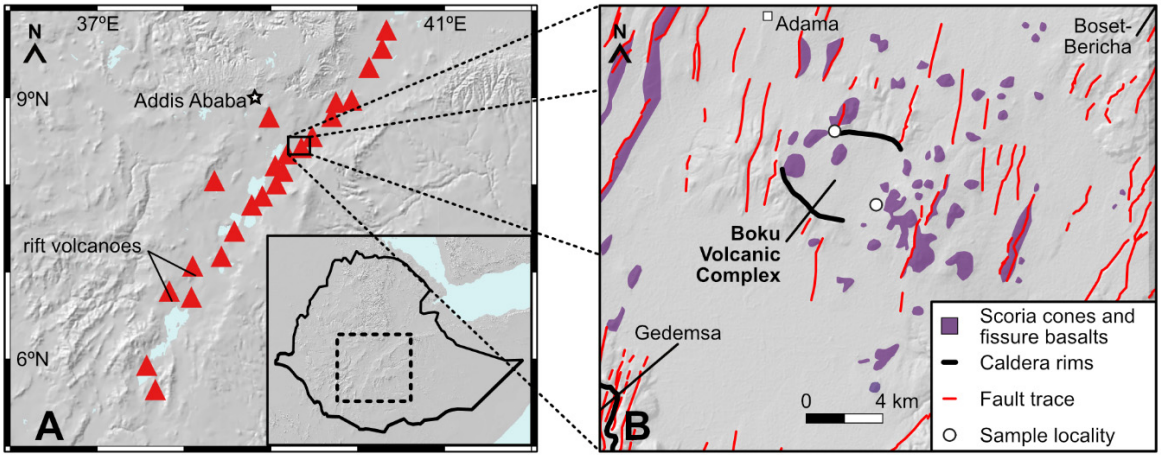

Fig. 1. (left) Map of the MER. (right) Map of the Boku Volcanic Complex.

The Main Ethiopian Rift (MER, Fig. 1) is a late-stage continental rift which has been extensively studied through geophysical approaches [2], which suggest that significant magmatic intrusion has occurred in rifting lithosphere. As much as half of the crustal volume may now comprise new igneous material [5,7]. The compositional and thermal effects of magma intrusion may modify the response of the Ethiopian crust to extension, determining where and how strain is localised as rifting proceeds [3]. Furthermore, degassing of these intruded melts during and after emplacement contributes to the significant diffuse CO_2 fluxes measured in the MER [8].

Strategy

In this study we investigate the storage depths and compositional diversity of intruded basaltic magmas in the northern MER using olivine-hosted melt inclusions (MIs). Olivine phenocrysts were picked from disaggregated scoria sampled from the Boku Volcanic Complex (Fig. 1), a collapsed silicic caldera system in the MER which hosts post-caldera basaltic scoria cones [9]. Scoria is preferred to lava to minimise volatile loss from MIs during cooling; however a significant number of MIs have cooled and degassed some volatiles to form a shrinkage bubble [10]. Olivine crystals were mounted on glass slides, polished to within 100 µm of the MI, and their MI vapour bubbles were analysed by Raman spectroscopy at the University of Cambridge. After further grinding and polishing to expose the inclusion, these crystals were mounted in epoxy for volatile and trace element analysis using Secondary Ion Mass Spectroscopy (SIMS) at the University of Edinburgh.

Results and discussion

Focussed mid-crustal intrusion in the Main Ethiopian Rift CO_2 concentrations in Boku MIs range from 35-5770 ppm in MI glass only. The subset of MIs for which CO_2 is determined in both glass and shrinkage bubble have total CO_2 contents of 1895-3248 ppm, with 15-46% of the CO_2 residing within the bubble. H_2O concentrations are less variable and have mean H2O of 1.1±0.2 wt%, discounting the three inclusions that have clearly degassed (≤0.4 wt% H_2O).

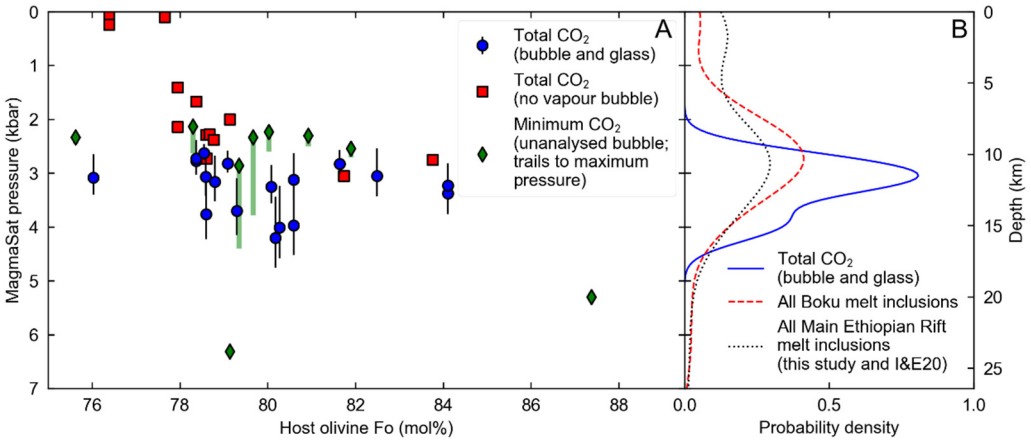

Fig. 2. (a) Solubility pressures for MER MIs determined via MagmaSat [11]. (b) Kernel density distributions for MIs with total CO_2 and glass CO_2 only [this study, 12].

Using the MagmaSat volatile solubility model (11) via VESIcal [13,14], we determine that saturation pressures for MIs where total CO_2 (bubble and glass) is determined have a relatively narrow pressure range from 2.5-4.5 kbar (~10-15 km, Fig. 2a). These pressures are among the deepest recorded volatile saturation depths for continental rift magmas. Pressures recorded by MER MIs without bubbles (this study, [6]; Fig. 2b) overlap partially with those with analysed bubbles, but their average CO_2 concentrations and therefore pressures are typically lower. These barometric results show a relatively limited distribution of magmatic storage depths, suggesting that a narrowly focussed zone of intrusion is present in the MER crust centred at ~12 km depth, coincident with the upper-lower crust boundary in the MER (7).

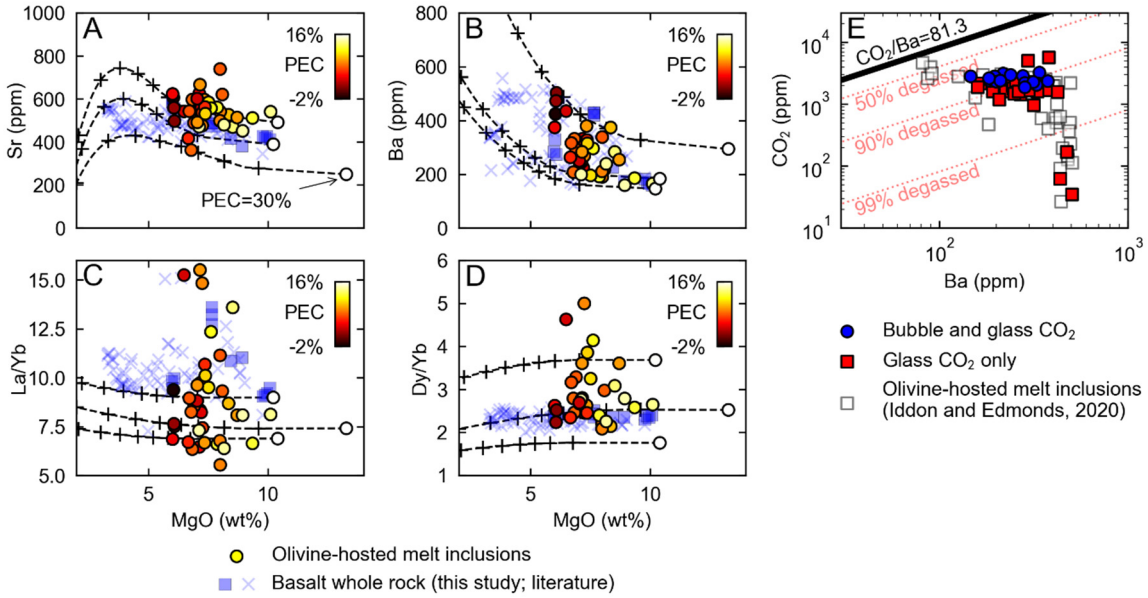

Fig. 3. (a-d) MI and whole rock trace element concentrations and trace element ratios plotted against MgO and liquid lines of descent (this study, [9,15]). (e) MI CO_2 plotted against Ba, primary CO_2/Ba of mid-ocean ridge basalt [16].

Diverse trace element compositions Incompatible trace element concentrations vary considerably in both MIs and lavas (Fig. 3A, B). Greater primary compositional variability is preserved in MIs over whole rocks, evidenced by variations in trace element ratios that are not significantly affected by fractionation (e.g., La/Yb, Dy/Yb, Fig. 3c, d). Physical interaction between intrusive bodies therefore appears to be limited. We infer that intruded magmas reside in a series of discrete sills emplaced at a common depth of 10-15 km (Fig. 4a). This is strongly supported by observations of the present-day MER crust ([15–18], Fig. 4b-c), and numerical models suggesting a mid-crustal ductile weak zone at these depths ([6], Fig. 4d).

CO_2 degassing from intruded melts By comparing CO_2 concentrations with trace elements of similar behaviour during mantle melting (e.g., Ba, Rb), CO_2 degassing from mantle melts can be assessed [16]. MIs clearly show evidence for degassing, even when total CO_2 is considered (Fig. 3e). Using CO2/Ba ratios of mid-ocean ridge basalts [16], we estimate that initial CO_2 ranges from 1-4 wt%, with ~60-95% of CO_2 having been exsolved in the mid crust during sill emplacement. The difference in CO_2 concentrations in primary mantle melts and those observed in our MI (2.0±0.6 wt%) is sufficient to match the observed CO_2 fluxes at the surface [8].

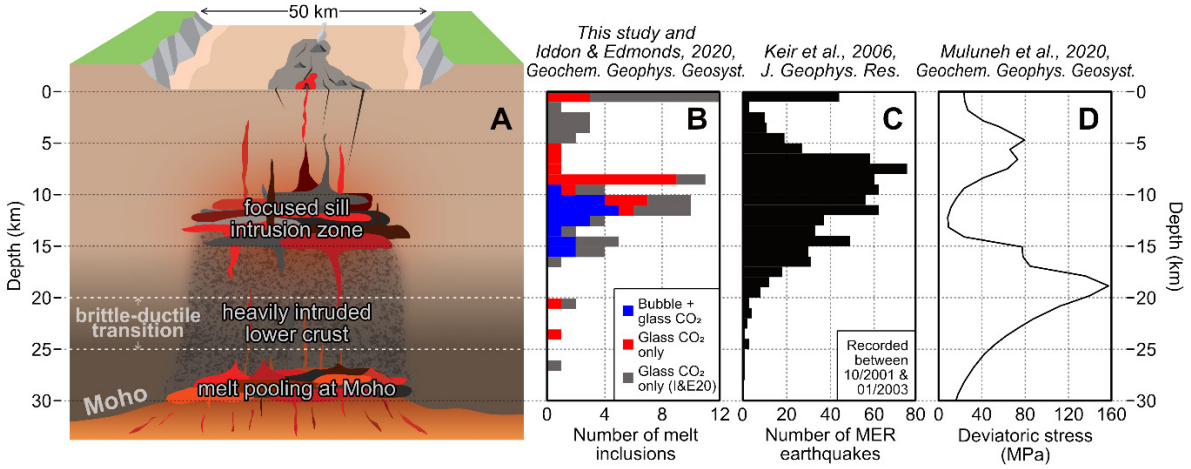

Fig. 4. (a) Summary cartoon illustrating our proposed structure of the MER crust. (b) Histogram of olivine-hosted MIs (this study, [14]). (c) Histogram of MER earthquakes [17]. (d) Numerical model of MER crustal deviatoric stress [6].

References

[1] White RS, et al., 2008. Nature 452(7186):460–4.
[2] Bastow ID, et al., 2011. Geological Society of America Special Paper 478, p. 51–76.
[3] Bastow ID, and Keir D, 2011. Nature Geoscience 4(4):248–50.
[4] Buck WR, 2006. Geological Society, London, Special Publications vol. 259, p. 43–54.
[5] Daniels KA, et al., 2014. Earth and Planetary Science Letters 385:145–53.
[6] Muluneh AA, et al., 2020. Geochemistry, Geophysics, Geosystems 21(7):e2020GC008935.
[7] Maguire PKH, et al., Geological Society, London, Special Publications vol. 259, p. 269–92.
[8] Hunt JA, et al., 2017. Geochemistry, Geophysics, Geosystems 18(10):3714–37.
[9] Tadesse AZ, et al., 2019. Journal of African Earth Sciences 149:109–30.
[10] Moore LR, et al., 2015. American Mineralogist 100(4):806–23.
[11] Ghiorso MS, and Gualda GAR, 2015. Contributions to Mineralogy and Petrology 169(6):53.
[12] Iddon F, and Edmonds M, 2020. Geochemistry, Geophysics, Geosystems 21(6):e2019GC008904.
[13] Iacovino K, et al., 2021. Earth and Space Science 8(11):e2020EA001584.
[14] Wieser PE,et al., 2022. Earth and Space Science 9(2):e2021EA001932.
[15] Nicotra E,et al., 2021. Scientific Reports 11(1):21821.
[16] Le Voyer M, et al. 2018. Geochemistry, Geophysics, Geosystems 20(3):1387–424.
[17] Keir D, et al., 2006. Journal of Geophysical Research: Solid Earth 111(B5).
[18] Cornwell DG, et al., 2006. Geological Society, London, Special Publications vol. 259, p. 307–21.
[19] Whaler KA, Hautot S., 2006. Geological Society, London, Special Publications vol. 259, p. 293–305.
[20] Chambers EL, et al., 2021. Earth and Planetary Science Letters. 573:117150.